
Unterschrift Betreuer



TECHNISCHE
UNIVERSITÄT
WIEN

DIPLOMARBEIT

Designing and stabilizing a non-planar femtosecond
enhancement cavity to excite the nuclear transition of the
low energy isomer state of Thorium-229

Ausgeführt am

Atominstitut

der Technischen Universität Wien

unter der Anleitung von Univ.Prof. Dipl.-Phys. Dr.rer.nat. Thorsten
Schumm

durch

Jakob Fellingner

Pettneu am Arlberg 11a
6574 Pettneu am Arlberg

Datum

Unterschrift

Designing and stabilizing a non-planar
femtosecond enhancement cavity to excite the
nuclear transition of the low energy isomer state
of Thorium-229

Masterthesis
Jakob Fellingner

Institute of Atomic and Subatomic Physics,
overseen from Univ.Prof. Dipl.-Phys. Dr.rer.nat. Thorsten
Schumm

Kurzfassung

Diese Diplomarbeit beschäftigt sich mit der Kopplung eines optischen Frequenzkammes an einen Verstärkungs-Resonator. Dabei wird auf die Funktionsweise eines Verstärkungs-Resonators eingegangen. Weiters werden verschiedene Möglichkeiten aufgezeigt, einen solchen Resonator experimentell umzusetzen und die Vor- und Nachteile der verschiedenen Bauformen analysiert. Des Weiteren wird erläutert, welche Punkte für die Leistung entscheidend sind, die sich in dem Resonator aufbaut, und welche Schritte nötig sind, um den Resonator stabil mit dem Frequenzkamm zu koppeln und auf Resonanz zu stabilisieren.

Abstract

This master thesis deals with the coupling of an optical frequency comb to an enhancement cavity. The operation principle of an enhancement cavity will be explained, and different ways to build such a cavity will be discussed. It will also be shown which parameters are critical to get the highest possible intensity, how to couple the cavity to the frequency comb and stabilize it on resonance.

Contents

1	Introduction and Motivation	1
1.1	Thorium-229	1
1.2	The Frequency Comb	2
1.3	High Harmonic Generation	4
2	Enhancement Cavity	5
2.1	Operation Principle	5
2.2	Enhancement Cavity with Dispersion and a Frequency Comb	10
2.3	Cavity Design	15
2.4	Transversal Cavity Modes	26
3	Coupling and locking a Frequency Comb to an enhancement Cavity	29
3.1	Mode Matching	29
3.2	T.W. Hänsch and B. Couillaud Stabilization	32
4	Implementation	37
4.1	Optical Setup Overview	37
4.2	Planar Ring-Cavity Setup	37
4.3	3D-Cavity Setup	39
4.4	Aligning a Ring-Cavity	41
4.5	Hänsch Couillaud Stabilization Setup	43
4.6	Connection of the Cavity and the Optical Table	43
4.7	Reconditioning the 3D-Cavity	48
4.8	Final Stability and Possible Further Improvements	53
5	th Harmonic	57
6	Summary and Outlook	59
A	Components	62

1 Introduction and Motivation

The radio isotope Thorium-229 shows a remarkable and unique property: it possesses an extremely low-energy excited isomer state of the nucleus which is expected around $7.6 \pm 0.5 \text{ eV}$ [1].

1.1 Thorium-229

The theoretically predicted energy levels of Thorium (close to the ground state) can be seen in Fig. 1.1. The energy of 7.6 eV corresponds to laser light in the 160 nm region. The existence of such a low-energy nuclear state would make it possible to perform spectroscopy of the nucleus of Thorium-229 with laser light. By means of high-energy gamma spectroscopy of the higher excited states of the nucleus, the existence of this transition has been proven, and the energy of this transition was measured to $7.6 \pm 0.5 \text{ eV}$, see Fig. 1.2 [1]. Nevertheless, the exact wavelength has not been determined yet, also the lifetime remains unknown. Comparison with similar systems estimates it at around 1000 seconds . This means that the transition has a high energy and a narrow linewidth which makes the transition a promising candidate for a new frequency standard. It was first suggested by Peik that it could be possible to embed Thorium-229 in a crystal which is transparent in the ultraviolet regime [2]. This would make it possible to perform laser spectroscopy on the isomer state, which would allow building a solid-state optical clock. To excite the nuclear transition of the low-energy isomer state of Thorium-229, with a transition energy of approximately 7.6 eV , a laser source around 160 nm is needed. However, at the current state of research, no frequency tunable laser at this wavelength range exists. Different working groups around the world already

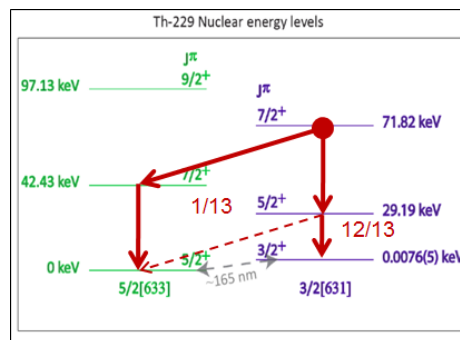


Figure 1.1: Th-229 Nuclear energy levels [1].

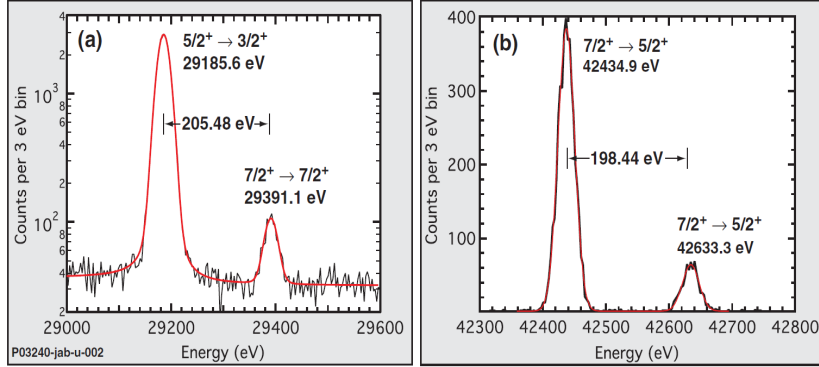


Figure 1.2: X-ray spectrometry (XRS) spectra in the 29 and 42 keV energy regions. Data illustrated for the 29 keV doublet (ΔE_{29}) (a), data illustrated for the 42 keV doublet (ΔE_{42}) (b). Black lines represent the data, red lines represent the least-square fitting results. Full-energy peaks are labeled by J^{Π} of the corresponding Th-229 transition [1].

used ultraviolet frequency combs for spectroscopy on atoms, see [3] [4] [5] [6]. There are strong hints at the possibility of using a frequency comb with a central wavelength of 800 nm, which will be introduced in Sec. 1.2, to excite the low-energy isomer state of Thorium-229. Therefore, the comb spectrum has to be shifted to the UV-regime to generate an ultraviolet frequency comb with a central wavelength of 160 nm. This is done by using high harmonic generation in Xenon, which will be explained in Sec. 1.3. High harmonic generation is a non-linear process. To reach a sufficient intensity, an enhancement cavity is needed. This master thesis deals with designing such a cavity, its coupling to the frequency comb and its stabilization.

1.2 The Frequency Comb

The frequency comb is a precision measurement tool for laser frequencies. It was invented by the group of Theodor Hänsch at the Max-Planck-Institute for Quantum-Optics in Munich [7]. Briefly described, it is a pulsed, mode locked laser with carrier-envelope phase stabilization. The pulses have a timescale on the femtosecond range and are sent with a repetition frequency of f_{rep} . The spectrum of such a pulse train consists of hundreds of thousands different frequencies. The spectrum of an infinite number of pulses has an infinite number of modes with a free spectral range of f_{rep} with a Gaussian envelope function, this can be seen in Fig. 1.3. It is shaped like a comb giving the frequency comb its name. The frequency comb sends a femtosecond pulse

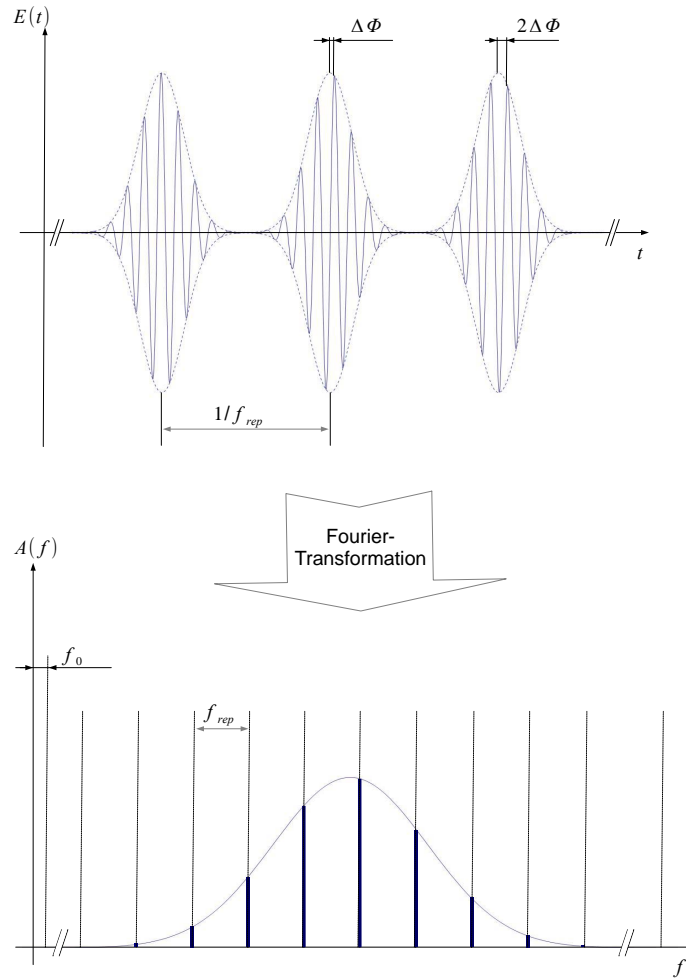


Figure 1.3: Spectrum of a frequency comb with a repetition frequency of f_{rep} . The spectrum of such a laser source has a spectral mode every f_{rep} .

continuously every $1/f_{rep}$. From pulse to pulse the underlying carrier gets a phase shift of $\Delta\Phi$. The spectrum of the comb starts at an offset frequency f_0 , which corresponds to the phase shift in the time domain and the repetition frequency $f_0 = \Delta\Phi f_{rep}/2\pi$. An arbitrary mode of the comb spectrum M_n is given by $M_n = f_0 + n f_{rep}$. A 800 nm central wavelength Titan Sapphire laser based frequency comb is used for this master thesis, see annex A.2. For more information about frequency combs see [7] [3].

1.3 High Harmonic Generation

High harmonic generation is a non-linear laser-matter interaction [8]. The basic model for laser-matter interactions is given by:

$$N\gamma + X \longrightarrow X^{q+} + qe^{-} + \gamma'. \quad (1.1)$$

The incoming photons $N\gamma$ interact with the atom X and produce multiply charged ions X^{q+} , photoelectrons qe^{-} and photons γ' . Such a non-linear coupling can lead to radiation and to high harmonic generation among others. High harmonic generation results from a non-linear parametric scattering process [8], which can be described by:

$$N\gamma(\omega) + X \longrightarrow \gamma'(N\omega) + X. \quad (1.2)$$

A high energy laser with the frequency ω can generate a radiation of the frequency $N\omega$. This radiation is called high harmonic radiation of the order of N . According to the electric-dipole approximation for a spatially homogeneous medium, N can only assume odd integer values [8]. This offers the possibility to generate laser light in the 160 nm range, by using the 5th harmonic of a 800 nm laser. This process has been well investigated in the past, see [8] [9] [10] [11]. The critical value for high harmonic generation is the intensity. It has been shown that Xenon is the one non-radioactive gas with the lowest required intensity for generating high harmonics, there are theoretical evidences that radon needs a little lower intensity, but no measurement data could be found [12]. However radon is a radioactive gas and therefore not suitable to use. Xenon still needs an intensity of $10^{13} \text{ W/cm}^2 \sim 10^{14} \text{ W/cm}^2$, as shown in Fig. 1.4 [11]. Such a high intensity cannot be reached by just focusing the light of a state of the art 800 nm laser. Therefore, it has to be enhanced in a cavity.

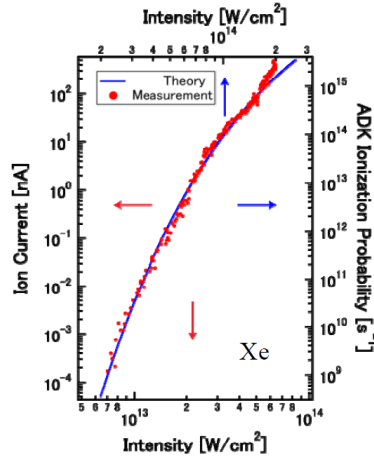


Figure 1.4: Measurement of the high harmonic signal intensity dependence in Xenon by Yohei Kobayashi [11].

2 Enhancement Cavity

To achieve the high peak power, to drive the high harmonic process at a repetition frequency of ~ 100 MHz, we utilize an enhancement cavity. An enhancement cavity is a Fabry-Perot interferometer built with the specific intention of boosting the intensity within the optical cavity to drive some non-linear process [5].

2.1 Operation Principle

To understand the operation principle of an enhancement cavity lets consider a system out of four mirrors which can be used as an enhancement cavity, see Fig. 2.1. If laser light from a continuous wave laser is sent to the first mirror, which is called in-coupling-mirror, some light will be reflected and some light will be transmitted through the mirror, depending on the different reflection indices of the mirror and the surrounding medium. This calculation resembles the calculation for multiple-beam interference in a Fabry-Perot interferometer and is found in [14]. The four mirrors are aligned in a way that the transmitted light travels from mirror-1 to mirror-2, from mirror-2 to mirror-3, from mirror-3 to mirror-4, and finally from mirror-4 back to mirror-1, ending at the starting point. This setup is called planar ring cavity and is the state of the art configuration for an enhancement cavity. The following calculations refer to a cavity in vacuum. To understand the advantage of using an enhancement cavity, to drive an inefficient non-linear process, like high harmonic generation, one has to calculate the electric field, which is build up in the cavity. If the incoming laser light has an electric field amplitude $E^{(i)}$, the amplitude after the transmission through the in-coupling-mirror $E^{(c)}$, which is the electric field amplitude in the cavity can be expressed by

$$E_1^{(c)} = E^{(i)}t_m, \quad (2.1)$$

where t_m is the transmission coefficient of the in-coupling-mirror. After one round trip, the light has been reflected three times in the cavity and one time at the in-coupling-mirror, the beam travels in the same direction as the incoming light. Note that the in-coupling-mirror plays a decisive role, therefore it is treated separately in the calculation. The electric field amplitude after one round trip can be calculated by

$$E^{(c)} = E^{(i)}t_m r_c r_m e^{i\varphi}, \quad (2.2)$$

where r_m is the reflection coefficient of the in-coupling-mirror, r_c is the reflection coefficient of all remaining parts of the cavity, which includes all losses in the cavity additional

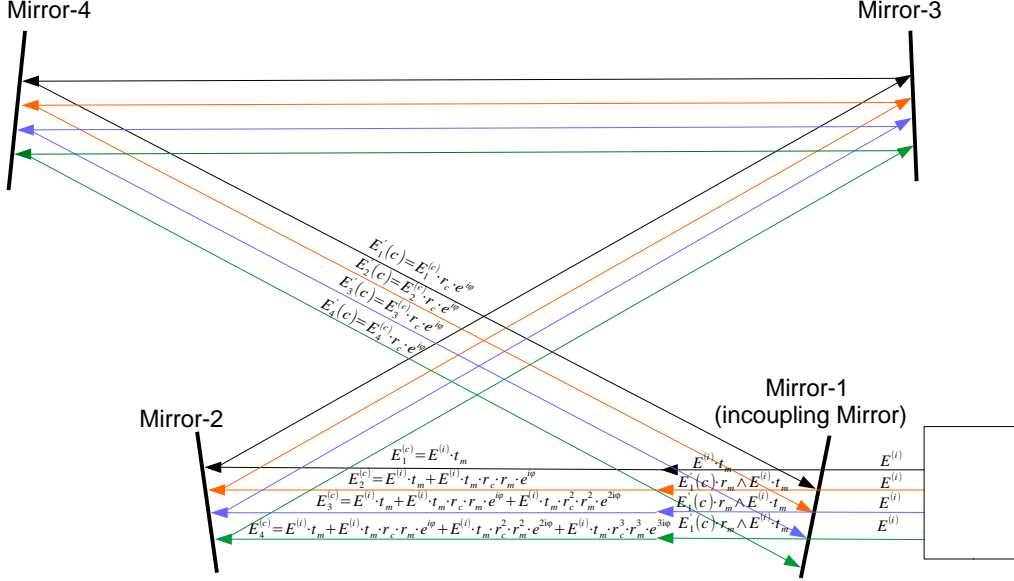


Figure 2.1: Calculating the electric field in the cavity, light transmits through the in-coupling-mirror, travels from mirror-1 to mirror-2, from mirror-2 to mirror-3, mirror-3 to mirror-4, and from mirror-4 back to mirror-1, ending at the starting point. It is superposed with the incoming light and again travels through the cavity. This is repeated infinite times to build up the cavity light field [13].

to the reflection losses. The parameter φ corresponds to a phase shift which is accumulated after one round trip. The round trip field is superposed with the incoming light and this leads to the intra-cavity field:

$$E_2^{(c)} = E^{(i)} t_m + E^{(i)} t_m r_c r_m e^{i\varphi}. \quad (2.3)$$

If one repeats the round trip for $E_2^{(c)}$ and again superposes it with the incoming light the intra-cavity electric field is given by:

$$E_3^{(c)} = E^{(i)} t_m + E^{(i)} t_m r_c r_m e^{i\varphi} + E^{(i)} t_m r_c^2 r_m^2 e^{2i\varphi}. \quad (2.4)$$

To get the electric field of a build up cavity one has to calculate the field for an infinite number of round trips:

$$E_\infty^{(c)} = E^{(i)} t_m \sum_{n=0}^{\infty} (r_c r_m e^{i\varphi})^n. \quad (2.5)$$

For real mirrors and cavities

$$r_m < 1, \quad r_c < 1, \quad (2.6)$$

otherwise they would amplify the light and generate power which is definitely not possible without a gain medium. Now one can use the geometric series to obtain the electric field from the build up cavity:

$$E_{\infty}^{(c)} = \frac{t_m}{1 - r_m r_c e^{i\varphi}} E^{(i)}. \quad (2.7)$$

Note, depending on how close r_m and r_c are to 1, this sum converges after few, several hundreds, or several thousand round trips, which means that the build-up time is quite different for different enhancements. This will be important later on. The next step is to calculate the intensity which is built up in the cavity. The intra-cavity intensity is an important indicator for generating high harmonic radiation:

$$I^{(c)} = E_{\infty}^{(c)} E_{\infty}^{(c)*} = \frac{T_i}{1 + R_m R_c - 2\sqrt{R_m R_c} \cos \varphi} I_i. \quad (2.8)$$

This can be brought to a convenient form with a little trick:

$$I^{(c)} = E_{\infty}^{(c)} E_{\infty}^{(c)*} = \frac{T_i}{1 + R_m R_c - 2\sqrt{R_m R_c} (\cos \varphi - \cos 0 + 1)} I_i, \quad (2.9)$$

By using

$$\cos(\alpha) - \cos(\beta) = -2 \sin(\alpha + \beta)/2 \sin(\alpha - \beta)/2, \quad (2.10)$$

the intensity can be written as:

$$I^{(c)} = \frac{T_i}{(1 - \sqrt{R_c R_m})^2} \frac{1}{1 + \frac{4\sqrt{R_c R_m} \sin^2(\varphi/2)}{(1 - \sqrt{R_c R_m})^2}} I_i. \quad (2.11)$$

Now to get an even more compact form, one defines the enhancement of the cavity η_{cav} , which is an unit-free value, and the coefficient-of-finesse F by:

$$\eta_{cav} = \frac{T_i}{(1 - \sqrt{R_c R_m})^2}, \quad (2.12)$$

$$F = \frac{4\sqrt{R_c R_m}}{(1 - \sqrt{R_c R_m})^2}. \quad (2.13)$$

Finally one gets the equation for the intensity in the build up cavity:

$$I^{(c)} = \eta_{cav} \frac{1}{1 + F \sin^2(\varphi/2)} I_i. \quad (2.14)$$

If one interprets the equation for $I^{(c)}$ one can see that $1/(1 + F \sin^2(\varphi/2))$ is periodic and oscillates between 1 and $1/(1 + F)$. The factor η_{cav} is, as already mentioned, the enhancement of the cavity. For $\varphi = 2\pi n$, where n is an integer number, the intra-cavity intensity is given by:

$$I^{(c)} = \eta_{cav} I_i. \quad (2.15)$$

If considering an input coupler with a reflectivity of 99.9% and a cavity with a reflectivity of 99.9%, η_{cav} becomes 1000. Thus, one gets a build up power of 1000 I_i . This shows

the high benefit of using an enhancement cavity for an inefficient process. To get the maximum of intensity one has to design the cavity to satisfy $\varphi = 2\pi n$. As already mentioned, φ is the phase shift of the light during one round trip in the cavity. It does not matter if the phase shift comes from propagation φ_p or from dispersion $\varphi_d(\omega)$. Thus φ can be written as:

$$\varphi = \varphi_p + \varphi_d(\omega). \quad (2.16)$$

The propagation phase shift is given by the angular frequency ω of the laser, the length of the cavity L_c and the speed of light c by:

$$\varphi_p = \frac{L_c \omega}{c}. \quad (2.17)$$

If one considers a cavity without dispersion the intensity is given by:

$$I^{(c)} = \eta_{cav} \frac{1}{1 + F \sin^2\left(\frac{L_c \omega}{2c}\right)} I_i. \quad (2.18)$$

To get the maximum intensity the length of the cavity L_c has to satisfy

$$\frac{L_c \omega}{2c} = 2\pi n, \quad (2.19)$$

but for a continuous wave (cw) laser pumped cavity it is obviously not the only solution since the intensity reaches a maximum every $\lambda/2$. For a cavity without dispersion one can now design the cavity for the property η_{cav} . This can be done by choosing the in-coupling-mirror and the cavity mirrors. One has to keep in mind that there will be additional losses from whatever process one drives within the cavity, for example a Xenon gas jet, an out-coupler glass plate, dust or anything else which may influence the electric field in the cavity. If one analyses the equation for η_{cav} there are two characteristics which can be summarized as the rules of enhancement cavity design:

- For given losses in the cavity it is always better to match the transmission of the in-coupling-mirror to the losses of the cavity. This is shown in Fig. 2.2.
- For a given in-coupling-mirror it is always better to make the reflectivity of the cavity as good as possible, as it can be seen in Fig. 2.3.

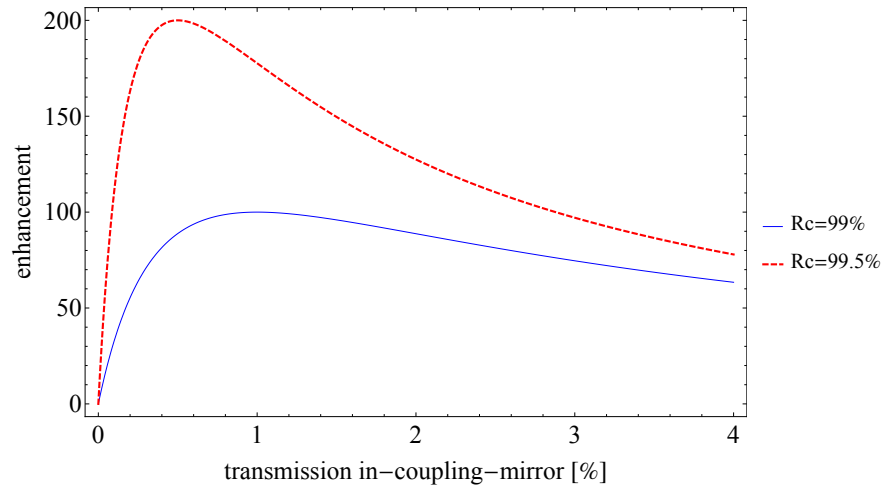


Figure 2.2: For given losses in the cavity it is always better to match the transmission of the in-coupling-mirror to the losses of the cavity. The red dashed line shows the calculated enhancement for a cavity with a reflectivity of 99.5%. There is a distinct maximum for the enhancement by a transmission of the in-coupling-mirror of 0.5%. The blue continuous line shows the calculated enhancement for cavity with a reflectivity of 99%, there is also a maximum of the enhancement when matching cavity losses and in-coupling transmission.

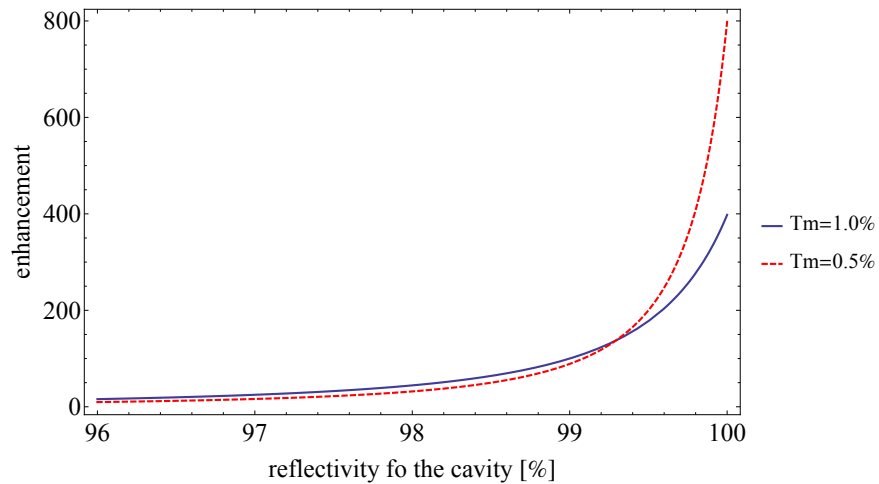


Figure 2.3: For a given in-coupling-mirror in the cavity, it is always better to make the reflectivity of the cavity as good as possible. If one calculates the enhancement for a given in-coupling-mirror it is continuously getting better, with higher reflectivity of the cavity. For low losses, the low in-coupling-mirror transition gives significantly better results, but for high losses, it is slightly better to have a high in-coupling-mirror transition. The break even point is exactly where the cavity losses reach the transition of the low transition in-coupling-mirror.

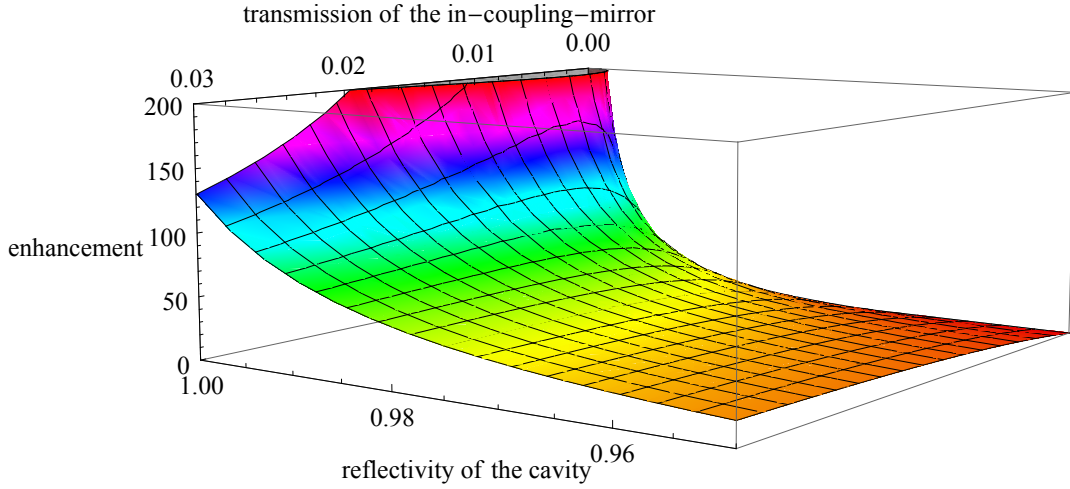


Figure 2.4: Dependence of the enhancement on the transmission of the in-coupling-mirror and the reflectivity of the cavity combined.

These two properties can be combined in a 3D-plot. It is quite useful to choose the correct parameters for a necessary enhancement by cutting through the plot at a given enhancement. This yields a surface with the possible parameters for the in-coupling-mirror and the cavity reflectivity, see Fig. 2.4. Things become more difficult if one does not pump the cavity with a cw-laser but with a pulse laser and includes a dispersion phase shift $\varphi_d(\omega)$ to the calculation, which is done in the next section.

2.2 Enhancement Cavity with Dispersion and a Frequency Comb

If the cavity is not pumped with a cw-laser but with a frequency comb, there are several additional things to be kept in mind. The spectrum of a pulsed laser source which sends the pulses with a repetition frequency of f_{rep} , as shown in Fig. 1.3, has a large number of spectral modes. The width of the complete spectrum is given by the pulse length. To enhance such a spectrum, every mode of the frequency comb should be enhanced in the cavity. If taking a closer look to Eq. 2.1 which was deduced for a cw-laser pumped cavity, and chooses $L_c = \frac{c}{2f}$, one gets a function with an periodicity of f . This means the cavity has a mode every f where light can be enhanced; the space between the modes is called 'free spectral range' $\Delta\nu_{FSR}$. For a frequency comb pumped cavity it is slightly different, the length of the cavity has to be $L_c = \frac{cn}{f_{rep}}$, where n is an integer number, to get a $\Delta\nu_{FSRPuls}$ of f_{rep} and enhance every comb mode [15]. Figure 2.5 shows this function for a repetition frequency of $f_{rep} = 108$ Mhz, with different in-coupling-mirror parameters T_m , $R_m = 1 - T_m$ and cavity reflectivity R_c . The cavity now also theoretically has an infinite number of spectral modes with a distance of f_{rep} . This means, that every comb mode exactly overlaps with one of these cavity modes and the complete comb spectrum is enhanced, see Fig. 2.6. Note, that for the cavity used during this master thesis, the

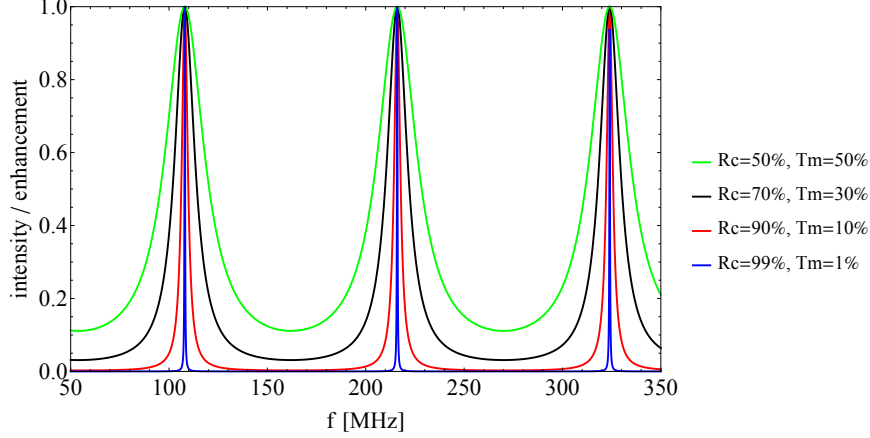


Figure 2.5: Repetition of the cavity spectral modes, for a pulsed laser pumped cavity. For $L_c = \frac{c}{f_{rep}}$, $\Delta\nu_{FSRPuls} = \frac{c}{L_c}$ is equal to the f_{rep} of the frequencycomb. The width of the modes depends on the parameter of the in-coupling-mirror and the cavity reflectivity. One can see that the width of the function broadens when the in-coupling-mirror and the cavity reflectivity get worse.

cavity length was set to $L_c = \frac{c}{f_{rep}}$. If one further considers not only the propagation phase φ_p , but also the dispersion phase $\varphi_d(\omega)$, things become more difficult. To analyze the influence of the dispersion phase, it is useful to Taylor-expand the ω dependent part of φ near a slightly different angular frequency ω' :

$$\varphi = \varphi_p + \varphi_{d0} + \varphi_{d1}(\omega - \omega') + \varphi_{d2}(\omega - \omega')^2 + O(\omega - \omega')^3. \quad (2.20)$$

If one starts with a pulse as shown in Fig.2.7(a) and adds the shift of φ_d which is done by Fourier-transforming the pulse into the angular frequency domain, adding the ω -dependent phase shift and transforming it back into the time domain, the influence of the different Taylor terms of $\varphi_d(\omega)$ on the pulse can be observed. For a non-zero φ_{d0} the pulse has the same envelope but a shifted underlying carrier frequency, see Fig.2.7(b). The φ_{d1} part shifts the complete pulse, but the shape of the envelope and the underlying carrier frequency are not changed, as shown in Fig.2.7(c). The φ_{d2} term will broaden and distort the pulse, according to Fig.2.7(d). Higher order Taylor terms are ignored in this calculation. The phase shift of the linear term of $\varphi_d(\omega)$ is given by:

$$\varphi_{dlin}(\omega) = \varphi_{d0} + \varphi_{d1}\omega - \varphi_{d1}\omega'. \quad (2.21)$$

As shown in Fig.2.7, $\varphi_{dlin}(\omega)$ shifts the complete pulse as well as the underlying-carrier-frequency. The pulses sent from the frequency comb have a shifted underlying-carrier-frequency of $\Delta\Phi$ from pulse to pulse. The frequency shift corresponds to the offset frequency f_0 and the repetition frequency f_{rep} of the comb by:

$$\Delta\Phi = \frac{f_0 2\pi}{f_{rep}}. \quad (2.22)$$

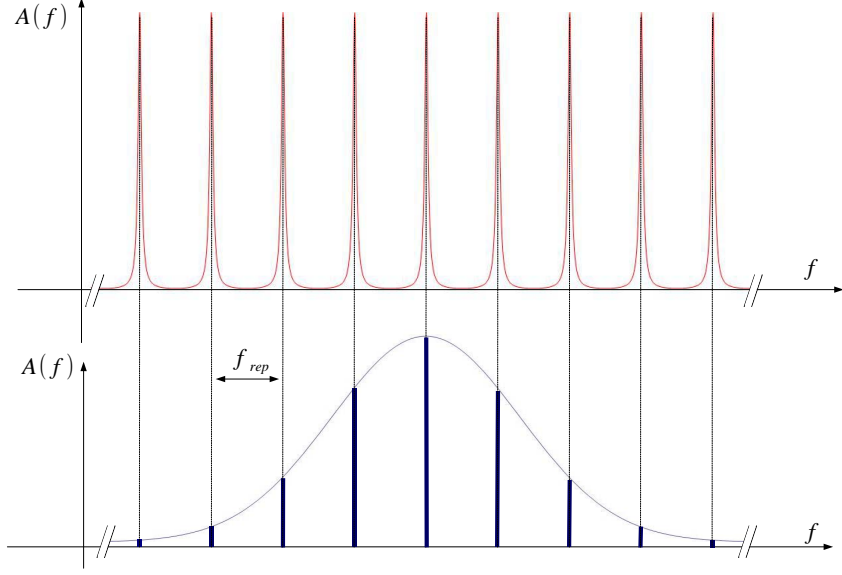


Figure 2.6: If the propagation phase shift is matched to the cavity length and the low order dispersion is compensated by tuning the cavity length and the comb offset, the spectral cavity modes overlap with the comb modes. The whole frequency comb is enhanced in the cavity and can be used for high harmonic generation.

Now $\varphi_{lin}(\omega)$ can be compensated by choosing the right comb offset frequency f_0 and changing the cavity length by δL_c . The phase shift imposed by a change of the cavity length δL_c is given by:

$$\varphi_{\delta L_c}(\omega) = \frac{\delta L_c \omega}{c}. \quad (2.23)$$

Such a compensation is feasible if there is a suitable solution for f_0 and δL_c :

$$\Delta\Phi(f_0) + \varphi_{\delta L_c}(\omega) = -\varphi_{lin}(\omega). \quad (2.24)$$

This yields:

$$\frac{f_0 2\pi}{f_{rep}} + \frac{\delta L_c \omega}{c} = -(\varphi_{d0} + \varphi_{d1}\omega - \varphi_{d1}\omega'). \quad (2.25)$$

The angular frequency ω of comb mode n is given by:

$$\omega(n) = (f_0 + n f_{rep}) 2\pi. \quad (2.26)$$

Inserting Eq. 2.26 in Eq. 2.25 yields:

$$\frac{f_0 2\pi}{f_{rep}} + \frac{\delta L_c 2\pi f_0}{c} + \frac{\delta L_c n 2\pi f_{rep}}{c} = -(\varphi_{d0} + \varphi_{d1} 2\pi f_0 + \varphi_{d1} n 2\pi f_{rep} - \varphi_{d1}\omega'). \quad (2.27)$$

This has to be fulfilled for every n to enhance every comb mode again. By equating coefficients δL_c and f_0 can be determined to:

$$\delta L_c = -\frac{\varphi_{d1}}{c}, \quad (2.28)$$

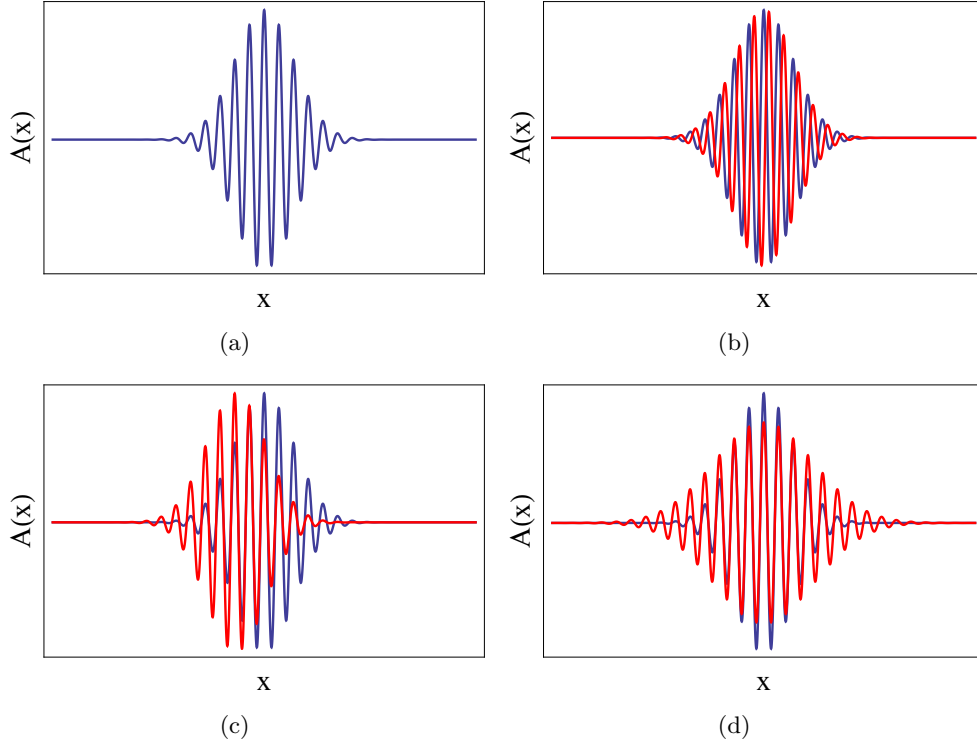


Figure 2.7: Pulse before any phase-shift (a), φ_{d0} shifts the underlying carrier frequency of the pulse but letting the pulse envelope unchanged (b), φ_{d1} shifts the complete pulse without changing the shape of the envelope and the underlying-carrier-frequency (c), φ_{d2} broadens and distorts the pulse (d). Higher order Taylor terms are ignored in this calculation.

$$f_0 = -\frac{\varphi_{d0} - \varphi_{d1}\omega'}{2\pi\left(\frac{1}{f_{rep}} + \frac{\delta L_c}{c} - \varphi_{d1}\right)}. \quad (2.29)$$

This adjustment of the comb offset frequency and the cavity length enables to enhance the complete comb spectrum, even for linear dispersion in the cavity. One does not really have to care about the absolute numbers, it is just important that the linear dispersion effects can be compensated. In Sec. 3.2, it will be shown that this compensation can be done by using the T.W. Hänsch and B. Couillaud stabilization method which also is explained in Sec. 3.2. However, Eq. 2.27 shows, that by tuning the cavity length and the comb offset frequency a quadratic or higher order phase shift ω cannot be compensated. This higher order dispersion leads to a counterintuitive behavior of the cavity.

For achieving the highest possible overall intensity for a cw-cavity, it is necessary to make sure that the reflectivity of the cavity is as large as possible and to match the transmission of the in-coupling-mirror to it. This does not affect the spectral match of the cw-laser to the cavity spectral modes. The only limit is the reflectivity of modern cavity mirrors and the stability of the built cavity. For a cavity with higher order dispersion which is pumped by a frequency comb this is different, since the cavity modes

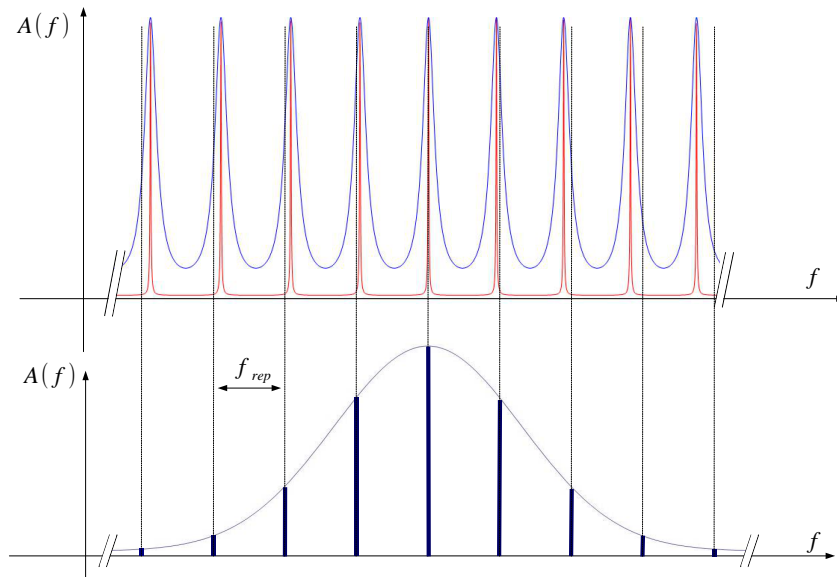


Figure 2.8: Cavity modes with higher order dispersion are shifted frequency square dependent, this cannot be compensated by any change of cavity length or comb offset. As a consequence, only a part of the comb spectrum is enhanced in the cavity. The cavity is filtering the comb spectrum. The red cavity spectrum is from a cavity with high reflectivity, the blue spectrum is from a cavity with low reflectivity, thus making the modes broader. The cavity with the broader spectral modes has a lower enhancement factor, but since it is also not that sensible to the phase-shift, it altogether may have more intra-cavity power.

are shifted due to dispersion. Thus, only a part of the comb spectrum can be enhanced in the cavity as it can be schematically seen in Fig. 2.8. The cavity is filtering the comb spectrum. Depending on the width of the spectral modes of the cavity and the value of the high order dispersion there is a limited frequency range Δf_c for which the comb modes couple energy into the cavity. High cavity reflectivity with matched transmission of the in-coupling-mirror makes the cavity spectrum mode quite narrow. This yields a narrow Δf_c and the overall power in the cavity becomes quite low. For low cavity reflectivity the cavity spectral modes becomes broader and a broader part of the comb spectrum is enhanced; an effect which may increase the power in the cavity. However, low cavity reflectivity means that the enhancement for the incoupled spectrum decreases. This is a min-max-problem. Figure 2.9 shows how a spectral cavity mode looks like for different cavity parameters. Nevertheless, it does not make sense to spend too much time thinking about optimizing the cavity for higher order dispersion before actually building it. Instead one should be able to identify the problem and solve it, by using some suitable chirped mirrors, for example.

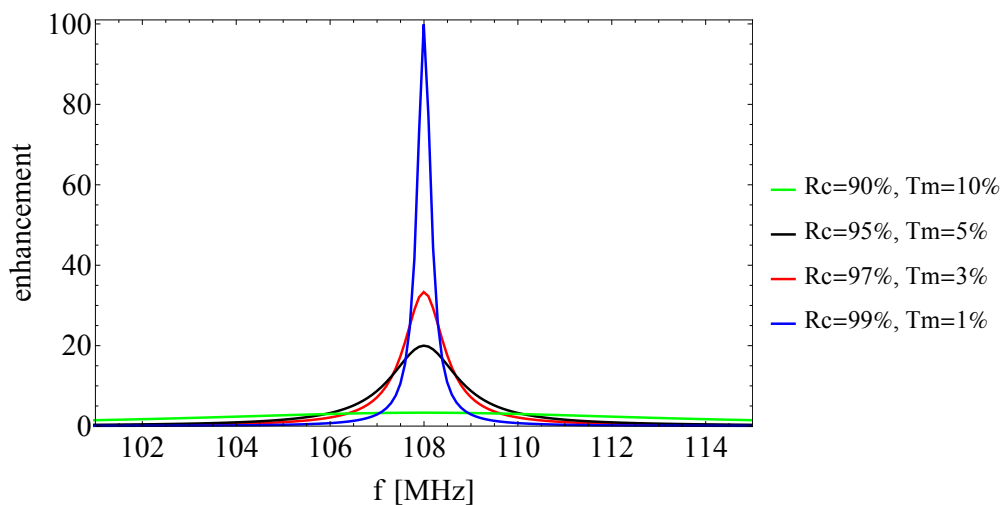


Figure 2.9: Enhancement depending on different cavity parameters. High cavity reflectivity means high enhancement, but a quite narrow cavity mode width, low cavity reflectivity means low enhancement, but a broadened cavity mode width.

2.3 Cavity Design

To generate high harmonics in Xenon, the intensity is the critical indicator. It is not enough to have high power in the cavity but also to focus the power to a small volume. This section will show how a cavity with the highest possible intensity can be designed. As shown in Sec. 2.1, one should match the length of the cavity to the repetition frequency of the pulsed laser source. There are several ways to design such a cavity. The first and simplest one is a linear cavity with just two mirrors. However, there are many disadvantages in using such a setup. In order to focus the beam in the cavity to a small diameter, it is common to couple a converging beam into the cavity and use two curved cavity mirrors, rather than sending a parallel beam into the cavity and use plane cavity mirrors. The distance between the two curved mirrors and the focal length of them must satisfy the stability criteria for cavities, which will be explained later on in this section. Depending on repetition frequency of the used frequency comb such mirrors may not exist and even if they do there would be no degree of freedom to tune the cavity length and the focus size of the cavity independently. Another disadvantage of a linear cavity is that the losses, which come from the setup to generate high harmonics and couple them out, will be increased because the beam hits it twice every cavity round trip. This would decrease the enhancement dramatically. The most common type of cavity for this task is the planar ring cavity, as discussed in Sec. 2.1, to calculate the intensity which is build up in an enhancement cavity. The beam path with a converging beam and two curved cavity mirrors with a radius of R can be seen in Fig. 2.10. The incoming beam is focused in f_2 . Note, that this focus is called f_2 because there is a second focus at f_1 , which has a smaller diameter and is used to generate the high harmonics. After f_2 the beam is divergent and becomes quite large on the curved cavity mirror. This curved cavity mirror focuses the beam in f_1 , and so on. To understand how the focus size and

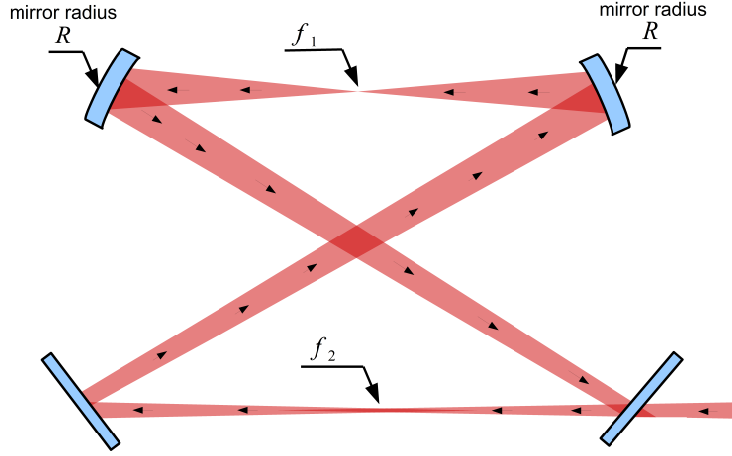


Figure 2.10: To get a small focused beam in the cavity a converging beam is send into the cavity and two curved cavity mirrors with an radius of R are used. The incoming beam is focused in f_2 , after f_2 the beam is divergent and is focused again by a curved mirror at f_1 . After f_1 the beam again is divergent and is focused again by a curved mirror at f_2 , and so on.

the stability range for this type of cavity is calculated, the ring cavity is simplified to a theoretical model as it can be seen in Fig. 2.11. Just two curved cavity mirrors with radius R are used with a distance d and instead of being reflected directly between the two mirrors the beam travels in one direction, the longer distance $L_c - d$, where L_c is the complete length of the cavity, to match the cavity length to the repetition frequency. Also important to note is, that the angle of incidence at the mirrors is zero. As already mentioned, this is just a theoretical model. To calculate the stability range of the cavity and the focus size, the Gaussian beam propagation and the ABCD-matrix calculus are used [13] [16]. The ABCD-Matrix for one cavity round trip starting and ending at focus f_1 is given by:

$$\begin{pmatrix} A_{f_1} & B_{f_1} \\ C_{f_1} & D_{f_1} \end{pmatrix} = \begin{pmatrix} 1 & d/2 \\ 0 & 1 \end{pmatrix} \begin{pmatrix} 1 & 0 \\ -2/R & 1 \end{pmatrix} \begin{pmatrix} 1 & L_c - d \\ 0 & 1 \end{pmatrix} \begin{pmatrix} 1 & 0 \\ -2/R & 1 \end{pmatrix} \begin{pmatrix} 1 & d/2 \\ 0 & 1 \end{pmatrix}. \quad (2.30)$$

For the focus f_2 the ABC-Matrix becomes:

$$\begin{pmatrix} A_{f_2} & B_{f_2} \\ C_{f_2} & D_{f_2} \end{pmatrix} = \begin{pmatrix} 1 & (L_c - d)/2 \\ 0 & 1 \end{pmatrix} \begin{pmatrix} 1 & 0 \\ -2/R & 1 \end{pmatrix} \begin{pmatrix} 1 & d \\ 0 & 1 \end{pmatrix} \begin{pmatrix} 1 & 0 \\ -2/R & 1 \end{pmatrix} \begin{pmatrix} 1 & (L_c - d)/2 \\ 0 & 1 \end{pmatrix}. \quad (2.31)$$

If the ABCD-Matrix is known one can calculate the propagation of a complex beam

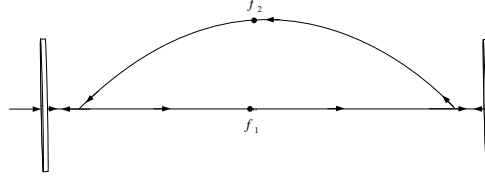


Figure 2.11: Simplified ring cavity model, just two curved cavity mirrors with radius R and a distance d . The beam travels in one direction for a longer distance $L_c - d$ to match the cavity length to the representation frequency; the angle of incidence at the mirrors is zero.

parameter $q(z)$ through the cavity. $q(z)$ is defined as

$$q(z) = z - iz_0, \quad (2.32)$$

with

$$z_0 = \frac{\pi\omega_0}{\lambda}, \quad (2.33)$$

where ω_0 is defined as the radius of the beam waist and λ is the wavelength of the laser. The propagation of q to a new beam parameter \tilde{q} given by the ABCD-Matrix can be calculated using:

$$\tilde{q} = \frac{qA + B}{qC + D}. \quad (2.34)$$

For the cavity to be stable after one round trip, the old and the new beam parameter have to be the same, yielding a self consistent equation:

$$q = \frac{qA + B}{qC + D}. \quad (2.35)$$

For a cavity setup as shown in Fig. 2.11 the ABCD-Matrix is symmetric yielding $A = D$ and this equation can easily be solved by:

$$q = \sqrt{\frac{B}{C}}. \quad (2.36)$$

Figure 2.12(a) and Fig. 2.12(b) show the calculated horizontal and vertical foci of the two cavity foci f_1 and f_2 for a cavity length $L_c = 2.71$ m and a curved mirror radius of $R = 150$ mm, depending on the distance of the two curved mirrors. These figures also show the stability range of the cavity. If the imaginary parts of the beam waist (dotted lines) are non-zero, it is not a physical solution anymore and the cavity does not work at this position. Figure 2.12(a) and Fig. 2.12(b) also show, that the horizontal and

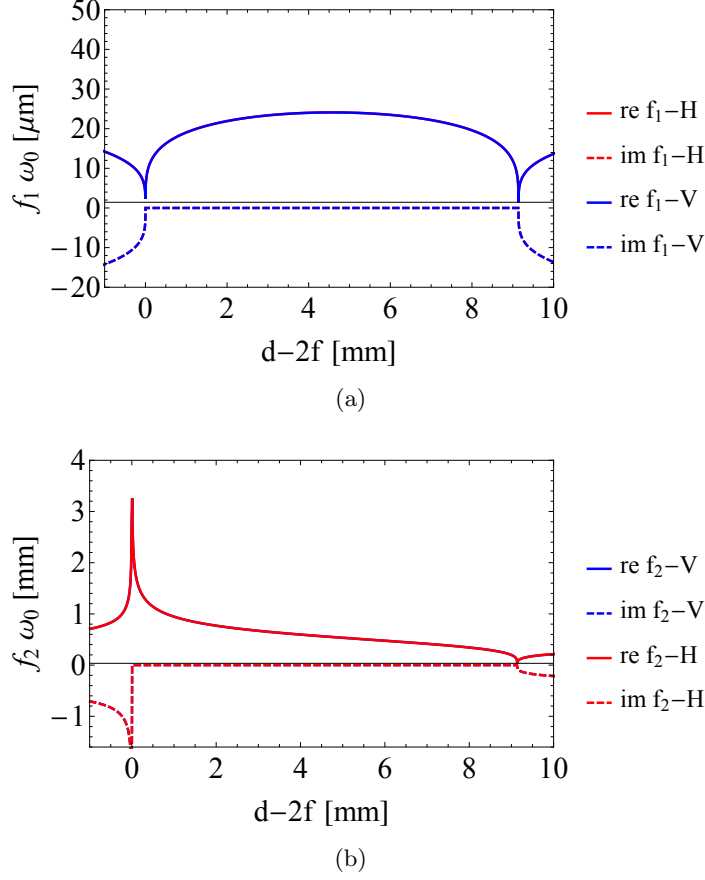


Figure 2.12: The calculated horizontal and vertical focus size of the two cavity focus f_1 (a) and f_2 (b), for a cavity length $L_c = 2.71$ m and a curved mirror radius of $R = 150$ mm depending on the distance of the two curved mirrors. The dotted lines show the imaginary parts of the beam waist. The cavity is stable, only for a vanishing imaginary part.

vertical foci exactly overlap, meaning that the horizontal and vertical foci have the same stability region. This happens because the angle of incidence on the curved mirror is theoretically set to zero and there is no difference in the calculation for the vertical and horizontal beam. However, to build a real ring cavity it is not possible to set the angle of incidence to zero and, as already explained, it is not suitable to use a linear cavity for high harmonic generation. The basic version of a real ring cavity is made out of four mirrors as shown in Fig. 2.14(a). Depending on how much space is available, the setup can be modified by adding more mirrors to make the setup more compact, on the other hand more reflections yield more cavity losses. Modern high reflector mirrors have a reflectivity of $R=99.999\%$ which means that the main cavity losses normally come from the high harmonic generation setup. To calculate the ABCD-Matrix for this setup, the horizontal and vertical focus must be treated differently because the angle of incidence on the curved cavity mirrors changes the focal length for the vertical and horizontal foci

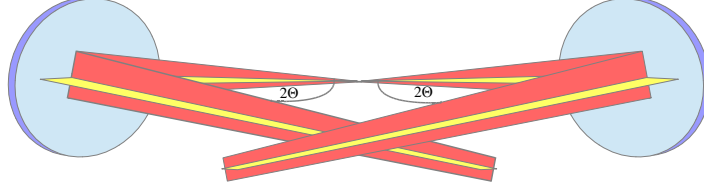


Figure 2.13: If the beam hits a curved mirror with an angle of incidence of $\theta/2$, the beam part parallel to the surface of incidence sees a mirror with a radius R of $R_{\parallel} = R \cos(\theta)$, and the perpendicular part of the beam sees a mirror with a radius R of $R_{\perp} = R/\cos(\theta)$, [17].

[17]. For a setup as shown in Fig. 2.13 the beam part parallel to the plane of incidence "sees" a mirror with a radius R_{\parallel} of

$$R_{\parallel} = R \cos(\theta), \quad (2.37)$$

and the beam part perpendicular to the surface of incidence sees a mirror with a radius R_{\perp} of:

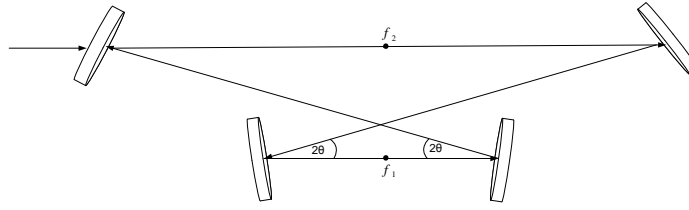
$$R_{\perp} = R/\cos(\theta). \quad (2.38)$$

This leads to new ABCD matrix for the two different cases:

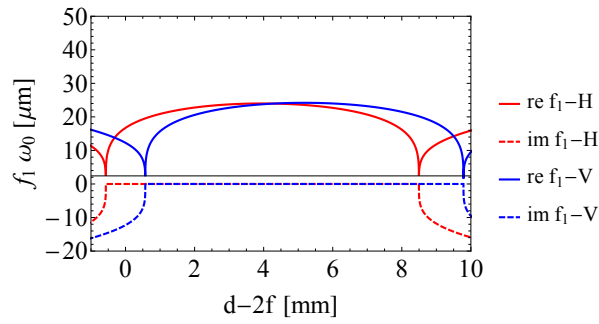
$$\begin{pmatrix} A_h & B_h \\ C_h & D_h \end{pmatrix} = \begin{pmatrix} 1 & \frac{d}{2} \\ 0 & 1 \end{pmatrix} \begin{pmatrix} 1 & 0 \\ -\frac{2\cos(\theta)}{R} & 1 \end{pmatrix} \begin{pmatrix} 1 & L_c - d \\ 0 & 1 \end{pmatrix} \begin{pmatrix} 1 & 0 \\ -\frac{2\cos(\theta)}{R} & 1 \end{pmatrix} \begin{pmatrix} 1 & \frac{d}{2} \\ 0 & 1 \end{pmatrix}, \quad (2.39)$$

$$\begin{pmatrix} A_v & B_v \\ C_v & D_v \end{pmatrix} = \begin{pmatrix} 1 & \frac{d}{2} \\ 0 & 1 \end{pmatrix} \begin{pmatrix} 1 & 0 \\ -\frac{2}{R\cos(\theta)} & 1 \end{pmatrix} \begin{pmatrix} 1 & L_c - d \\ 0 & 1 \end{pmatrix} \begin{pmatrix} 1 & 0 \\ -\frac{2}{R\cos(\theta)} & 1 \end{pmatrix} \begin{pmatrix} 1 & \frac{d}{2} \\ 0 & 1 \end{pmatrix}. \quad (2.40)$$

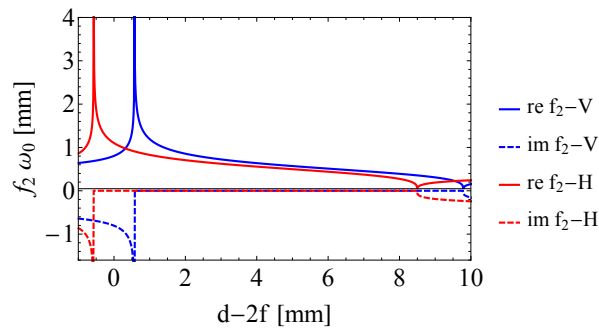
If the size of the two foci is once again calculated depending on the distance of the to focusing mirrors, one obtains the curves for the two foci, shifted with respect to each other, seen in Fig. 2.14(b) and 2.14(c). Depending on the angle of incidence, also setups exist where the two stability ranges for the horizontal and the vertical beam are completely apart from each other. Some ring cavity setups use material to compensate the different influence at the focus as it was done in [6], but this results in more losses in the cavity.



(a)



(b)



(c)

Figure 2.14: Schematic setup for a ring cavity (a), size of the horizontal and vertical focus at the position f_1 depending on the distance of the two curved cavity mirrors (b). Due to the angle of incidence θ at the curved mirror the horizontal and vertical parts of the beam "see" different mirror radii R . This leads to a different stability range for the horizontal and vertical beam parts. Size of the horizontal and vertical focus at the position f_2 depending on the distance of the two curved cavity mirrors (c). The stability regions for these foci are also shifted.

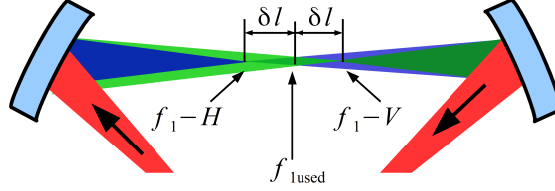


Figure 2.15: Shift $2\delta l$ between the position of the horizontal and vertical focus. The beam is utilized for high harmonic generation between the horizontal and vertical focus.

There is a third way to build such a cavity, it is called 3D-cavity. The angle of incidence at the first mirror is in the vertical plane and the emergent angle of the second curved cavity mirror is in the horizontal plane. Figure 2.16(a) shows a schematic setup. There has been no evidence that this type of cavity has ever been used to build an enhancement cavity. However, it has a large advantage which can be understood if the size and the stability range of the different foci are once again calculated. For the 3D-cavity the ABCD matrix for the first focus is given by

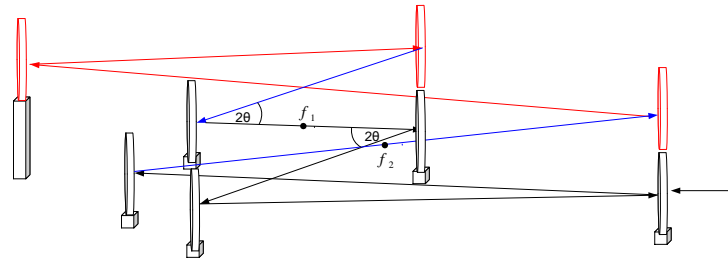
$$\begin{pmatrix} A_h & B_h \\ C_h & D_h \end{pmatrix} = \begin{pmatrix} 1 & \frac{d}{2} - \delta l \\ 0 & 1 \end{pmatrix} \begin{pmatrix} 1 & 0 \\ -\frac{2\cos(\theta)}{R} & 1 \end{pmatrix} \begin{pmatrix} 1 & L_c - d \\ 0 & 1 \end{pmatrix} \begin{pmatrix} 1 & 0 \\ -\frac{2}{\cos(\theta)R} & 1 \end{pmatrix} \begin{pmatrix} 1 & \frac{d}{2} + \delta l \\ 0 & 1 \end{pmatrix}, \quad (2.41)$$

$$\begin{pmatrix} A_v & B_v \\ C_v & D_v \end{pmatrix} = \begin{pmatrix} 1 & \frac{d}{2} + \delta l \\ 0 & 1 \end{pmatrix} \begin{pmatrix} 1 & 0 \\ -\frac{2}{R\cos(\theta)} & 1 \end{pmatrix} \begin{pmatrix} 1 & L_c - d \\ 0 & 1 \end{pmatrix} \begin{pmatrix} 1 & 0 \\ -\frac{2\cos(\theta)}{R} & 1 \end{pmatrix} \begin{pmatrix} 1 & \frac{d}{2} - \delta l \\ 0 & 1 \end{pmatrix}, \quad (2.42)$$

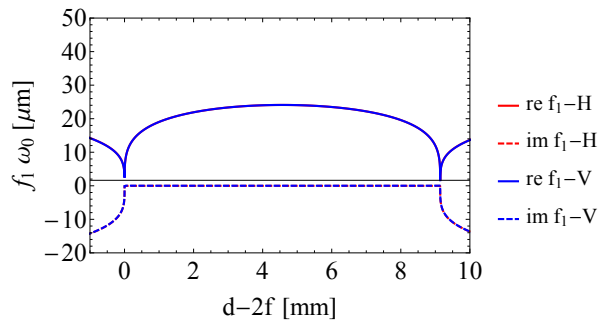
where δl has to be added to get a stable solution. These two matrices are not symmetric any more. Thus, for the calculation of q one has to solve the quadratic equation:

$$q_{1,2} = -\left(\frac{D-A}{C}\right) \pm \sqrt{\left(\frac{D-A}{2C}\right)^2 + \frac{B}{C}}. \quad (2.43)$$

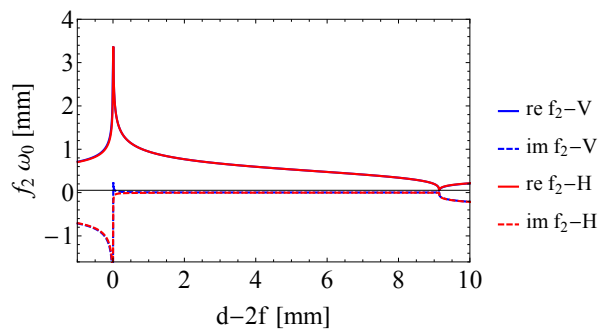
This leads to a result where the two foci f_1 and f_2 again overlap exactly, see Fig. 2.16(b) and 2.16(c). As a result, the possibility to use the cavity until the edge of stability, and gain a smaller cavity focus emerges. To get a non-imaginary solution, a shift $2\delta l$ between the position of the horizontal and vertical foci in the cavity has to be accepted, see Fig. 2.15.



(a)



(b)



(c)

Figure 2.16: Schematic layout for the 3D-cavity (a). Instead of having the angle of incidence and the emergence angle in the same plane, the angle of incidence is in the vertical and the emergence angle in the horizontal plane. The size of the horizontal and vertical focus at position f_1 as function of the distance of the curved cavity mirrors (b). As it can be seen the stability range for the horizontal and vertical focus completely overlaps, so with this set-up the cavity can be used until the edge of stability, furthermore f_2 overlaps completely (c)

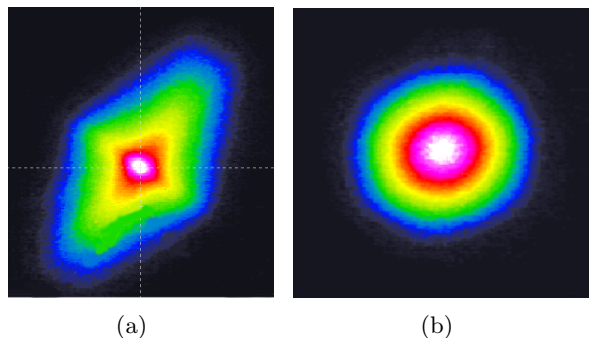


Figure 2.17: Beam profile of the second cavity focus of a planar ring cavity close to the edge of stability (a), beam profile of the second cavity focus of a 3D-cavity close to the edge of stability (b).

This means, that the focal spots for horizontal and vertical beam, depending on the cavity design, are a few microns apart from the centre of the two curved cavity mirrors. The 3D-cavity enables building a cavity where the whole theoretical stability region can be used. The only drawback by using the 3D-setup is that due to the asymmetric shift of the two foci, the beam has to be used between the horizontal and vertical focus, to get a round beam shape. This makes the beam larger, see Fig. 2.15. For a cavity with curved cavity mirror radius of $R = 150$ mm, a cavity length of $L_c = 2.771$ m and an angle of $\theta = 11.5$ degree, δl has a value of $\delta l = 225$ μm . For a cavity with a focus size of 10 μm , with the Gaussian beam propagation [13]

$$\omega(z) = \omega_0 \sqrt{1 + \left(\frac{z}{\pi \lambda \omega_0^2}\right)^2}, \quad (2.44)$$

and $z = 225$ μm , $\lambda = 800$ nm and $\omega_0 = 10$ μm the beam waist becomes 1.5 μm larger. This seems to be a disadvantage, but compared to a planar ring cavity one can use the cavity close to the edge of stability. This enables a significantly smaller beam even if it becomes slightly larger because of the asymmetry. The beam in the middle of the two foci where the high harmonic generation takes place has a nice shape, see Fig. 2.17(b). If the planar ring cavity is used, the beam at the edge of stability becomes quite asymmetric as it can be seen in Fig. 2.17(a). For getting a round beam by using a setup as shown in Fig. 2.14, we would have to use the setup with a beam diameter of nearly 25 μm . With the 3D-cavity a beam diameter of 12.5 μm can easily be reached, which results in an intensity that is four times higher. As a consequence, a significant difference in generating high harmonics is expected, as it can be seen in Fig. 1.4. To verify the calculations, the beam diameter of the focus f_1 is measured. Figure 2.18 shows the measurement setup. After the cavity focus f_1 the beam is coupled out by a pellicle in Brewster angle. With an imaging lens, the focus is imaged to a beam profiler. The magnification m of the image is given by,

$$m = \frac{l_b}{l_1 + l_2 + l_3}. \quad (2.45)$$

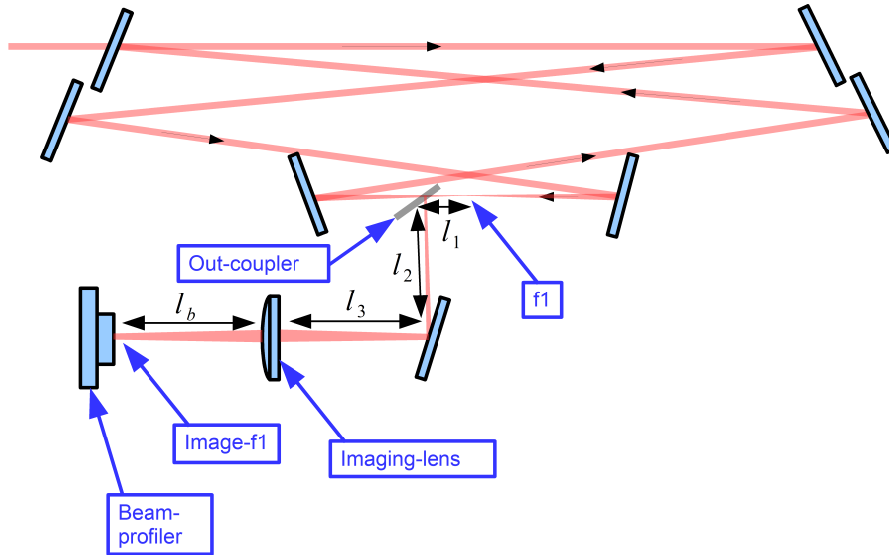


Figure 2.18: Setup for the measurement of the beam-diameter of focus f_1 . Light is coupled out of the cavity and magnified with a lens. The beam is measured with a beam-profiler.

For the measurement, the distance between the mirrors is changed by just moving one of the curved cavity mirrors. Since this shifts the focus, the beam profiler also has to be shifted for every measurement, to image the focus again. However, this also changes the magnification of the lens. In this measurement series, the magnification is taken as a constant. There are several possible measurement failures: First of all, it is not easy to measure the distance from the focus to the lens and also the distance from the lens to the beam-profiler, the beam has to hit the lens exactly in the middle and the lens surface has to be perpendicular to the beam, otherwise there is an imaging error. Furthermore, the out-coupler has to work correctly and also the alignment of the cavity has to be correct. Figures 2.19 and 2.20 show two different measurement series, made for two different in-coupling-beam-sizes. It can be seen that the cavity is usable until the edge of the stability region. For the measurement shown in Fig. 2.19 the beam waist of the horizontal and vertical beam behaves as calculated, within the limits of measurements accuracy. There is a small shift between the horizontal and vertical foci, this can be caused by the angle of incidence and emergence not being exactly the same. For the measurement shown in Fig. 2.20, within measurement accuracy it also shows a round beam, the outliers can be explained by bad alignment.

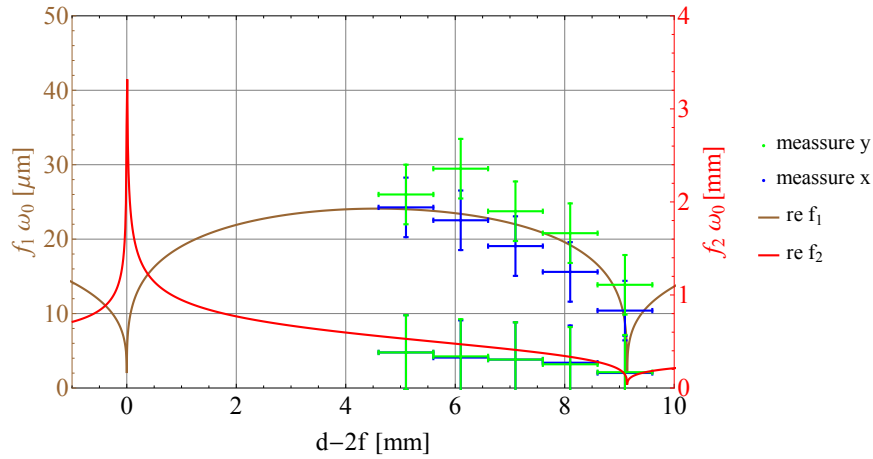


Figure 2.19: First measurement of the horizontal and vertical beam size of focus f_1 and f_2 . The brown curve shows the theoretical prediction for f_1 and the red curve shows the theoretical prediction for f_2 . The cavity is stable until near the edge of theoretical stability region. Within the accuracy of the measurements, the beam behaves as calculated.

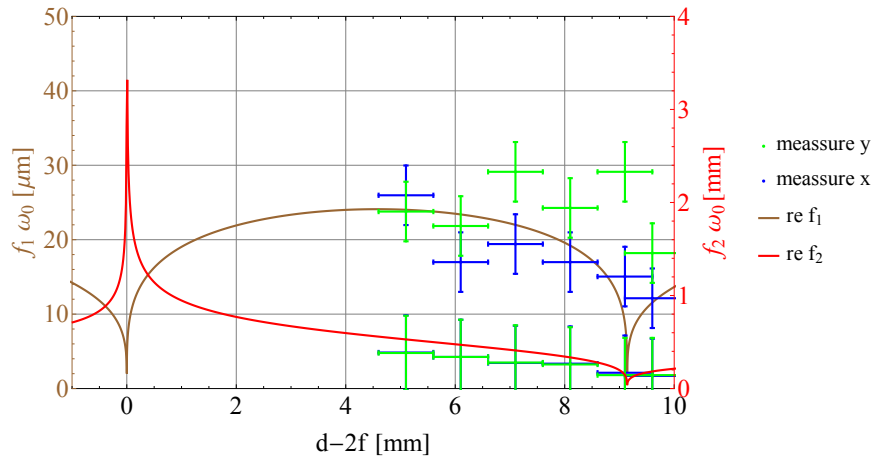


Figure 2.20: Second measurement of the horizontal and vertical beam size of focus f_1 and f_2 for a larger in-coupled beam. The brown curve shows the theoretical prediction for f_1 and the red curve shows the theoretical curve for f_2 . The horizontal beam diameter behaves as calculated. The vertical beam diameter within the accuracy of the measurements, except of one outlier, also follows the theoretical curve.

2.4 Transversal Cavity Modes

Laser beams are in many respects similar to plane waves; however, their intensity distributions are not uniform, but are concentrated near the axis of propagation and their phase fronts are slightly curved [16].

The electric field of coherent light satisfies the scalar wave equation [16]

$$\nabla^2 v + k^2 v = 0, \quad (2.46)$$

where \vec{k} is the wave vector and is described by:

$$k = \left| \vec{k} \right| = \frac{2\pi}{\lambda}. \quad (2.47)$$

For a wave which is travelling in the z -direction, Eq. 2.46 can be solved with the ansatz

$$v = \psi(x, y, z) e^{-ikz}, \quad (2.48)$$

which leads to:

$$\frac{\partial^2 \psi(x, y, z)}{\partial x^2} + \frac{\partial^2 \psi(x, y, z)}{\partial y^2} + \frac{\partial^2 \psi(x, y, z)}{\partial z^2} - 2ik \frac{\partial \psi(x, y, z)}{\partial z} = 0. \quad (2.49)$$

If one assumes that the variation in the z -direction is quite slow $\frac{\partial^2 \psi(x, y, z)}{\partial z^2}$ is negligible. Equation (2.49) can be solved by [16]

$$\psi(x, y, z) = e^{-i(P + \frac{k}{2q}(x^2 + y^2))}, \quad (2.50)$$

where P corresponds to a phase shift of the propagating light, and q is the complex beam parameter. Equation 2.50 shows a laser beam profile with a Gaussian beam shape perpendicular to the propagation direction and is called fundamental mode. It is the preferred mode for high intensity in the laser beam. Calculating the propagation behaviour yields

$$v(r, z) = \frac{\omega_0}{\omega} e^{-i(kz - \Phi) - r^2(\frac{1}{\omega^2} + \frac{ik}{2R})}, \quad (2.51)$$

where ω is the radius of the Gaussian beam at which the amplitude has dropped to $1/e$ of its maximum amplitude, ω_0 is the minimum diameter of the beam radius, $r^2 = x^2 + y^2$, $R(z)$ is the radius of the curvature of the wave front at position z , and Φ is a wavelength-dependent phase shift. There are also other solutions of the scalar wave equation which are called higher order modes [16]. An ansatz of

$$\psi(x, y, z) = g\left(\frac{x}{\omega}\right) h\left(\frac{y}{\omega}\right) e^{-i(P + \frac{k}{2q}(x^2 + y^2))}, \quad (2.52)$$

where $g = g(x, z)$, $h = h(y, z)$, are real functions, and $\omega = \omega(z)$ is the half width of a Gaussian beam which somehow scales the intensity pattern of the whole function leads to a differential equation of the form:

$$\frac{\partial^2 H_m}{\partial x^2} - 2x \frac{\partial H_m}{\partial x} + 2m H_m = 0. \quad (2.53)$$

Equation 2.53 is in fact the differential equation for the Hermite polynomial H_m of order m and leads to an infinite numbers of solutions for gh :

$$gh = H_m \left(\sqrt{2} \frac{x}{\omega} \right) H_n \left(\sqrt{2} \frac{y}{\omega} \right). \quad (2.54)$$

Such modes are called TM_{mn} modes with m, n integer numbers. The TM_{00} mode is the Gaussian beam mode. Some of the TM_{mn} modes which may appear in the cavity, are shown in Fig. 2.21. Equation 2.52 reveals that the higher order modes are products of the Hermite polynoms and the Gaussian function. The Hermite polynoms modulate the Gaussian function in the x - and y -direction. While the radius of curvature is the same for all modes, the phase shift Φ is different for every mode [16]:

$$\Phi(m, n, z) = (m + n + 1) \arctan \left(\frac{\lambda z}{\pi \omega_0^2} \right). \quad (2.55)$$

This mode dependent phase shift Φ is the reason why different modes need slightly different cavity lengths. If one modulates the cavity length and higher order modes appear in the cavity, resonance is reached at slightly different positions, see Fig. 2.22(a). There are several reasons why high order modes appear in the cavity:

- The cavity is not aligned correctly.
- There is no good mode matching.
- Vibrations miss align the cavity.
- There is some scattered light in the cavity caused by dust or dirt.
- The beam profile at the incoupled-beam is disturbed.

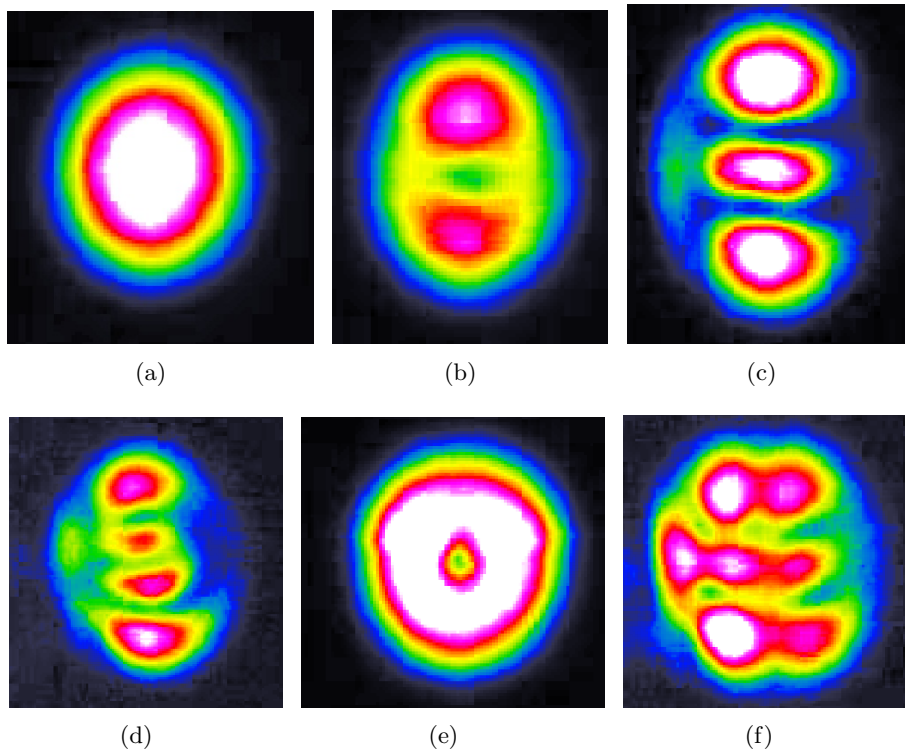


Figure 2.21: Some of the TM_{mn} modes appearing in the cavity. TM_{00} mode (a), TM_{01} mode (b), TM_{02} mode (c), Donut mode (e). Other appearing modes cannot be characterized exactly (f).

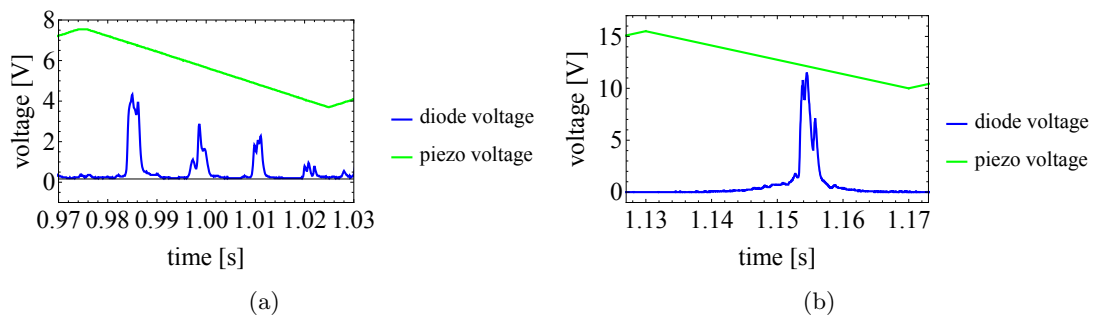


Figure 2.22: Modulation of the cavity length by driving a Piezo with a high voltage. If higher order modes appear in the cavity, they become resonant at slightly different cavity lengths (a), a scan over resonance from a cavity with no, or rather low intensity higher order modes (b).

3 Coupling and locking a Frequency Comb to an enhancement Cavity

3.1 Mode Matching

To couple a frequency comb to an enhancement cavity one has to calculate the beam parameter q of the cavity as explained in Sec. 2. The next step is to measure the beam profile of the frequency comb at two different points. This can be done with a beam-profiler or a razor blade on a translation stage. With the results of this measurement and the law of Gaussian beam propagation one can easily calculate the size and position of the beam waist. The difficult task is to design a system of lenses which focuses the beam exactly at the position of the cavity focus with the same waist size as the cavity waist. A good starting point for this calculation can be found empirically. As initial step the positions of f_1 and f_2 have to be calculated. Next step is to make an educated guess for a focal length of a lens or, if necessary for a system of lenses (note that every material in the beam adds dispersion that has to be compensated). Furthermore, a beam-profiler or a camera has to be placed in the second focus and the lens has to be arranged into a position where the beam on the camera is focused, see Fig. 3.1. The cavity, as already mentioned, is self-consistent meaning that after one cavity round trip the Gaussian beam parameter q stays the same for both foci but also after half a round trip the beam parameter of one focus changes to the beam parameter of the other focus. The result is that if the in-coming beam is focused at the second cavity focus, the first cavity focus also is aligned at the right position, just the quality of mode matching may not be good. To determine the mode matching the intra-cavity power at different cavity mirror distances is measured. Different cavity mirror distances

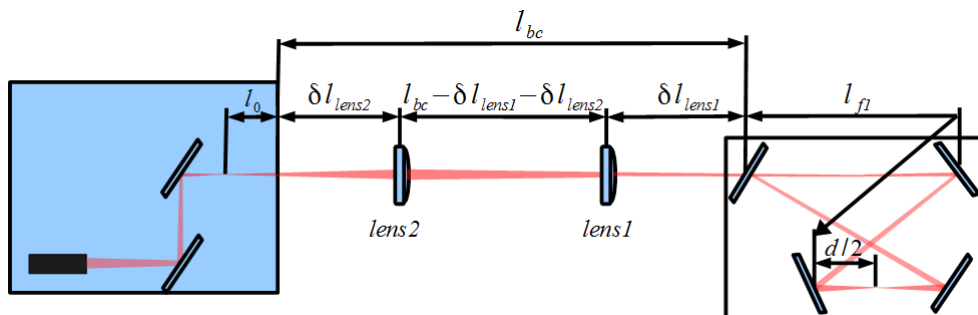


Figure 3.1: View of the setup to mode-match the frequency comb with the cavity. Two lenses used to get the optimal mode matching.

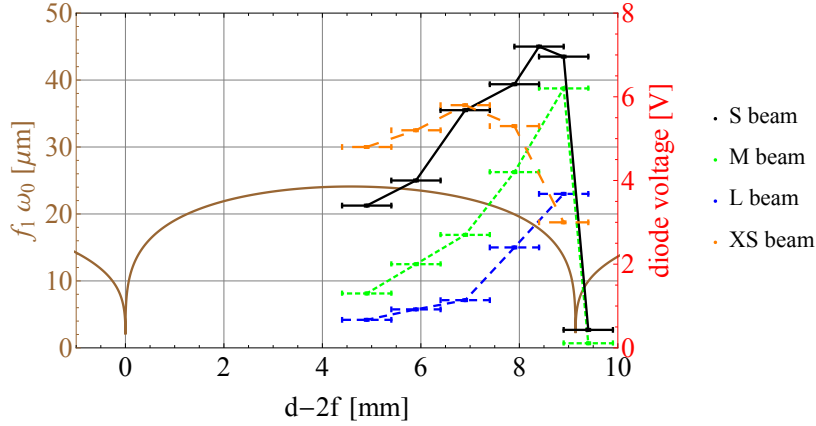


Figure 3.2: Measured intra-cavity power as a function of the distance of the curved cavity mirror for different incoming beams. For the large beam (blue curve) the highest power appears at the edge of stability of the cavity. Making the incoupled beam smaller which makes the focus larger, incouples more power in the cavity, but the maximum is still at the edge (green curve). An even smaller beam brings even more incoupled power (black curve), even smaller incoupled beam just shifts the best mode matching position to a larger focus size (yellow curve).

change the beam parameter q of the cavity, and also change the intra-cavity power as a function of the mode matching. If there is a maximum at the second part of the stable range of the cavity, mode matching is achieved and one can shift this maximum to the cavity focus size one needs by making the beam slightly larger or smaller. If there is no maximum, the distance or the focal length of the lens has to be changed. If the intra-cavity power in the middle of the stability curve is the largest (largest possible cavity focus), the focus of the incoming beam at f_1 is too large, and the size of the incoming beam has to be increased. For the highest power at the edge of stability (smallest possible cavity focus), the beam at f_1 is too small and thus, the incoming beam has to be smaller. This may be counter intuitive but it is essential to have a large beam on the curved cavity mirror, a small focus f_1 , a small beam on the curved cavity mirrors and a large focus f_1 . Four different lens systems were tested, and the power on resonance as a function of the mirror distance was measured, see Fig. 3.2. For the large beam (blue curve), the highest power appears at the edge of stability of the cavity. This may be an evidence that just some part of the incoming beam mode matches with the cavity focus, yielding a large intensity loss. If a 3D-cavity is used, the distance between the cavity mirrors can theoretically be enlarged towards the edge of stability. There the cavity beam gets arbitrarily small and the incoming beam is intended to match to the cavity focus. However, depending on the angle of incidence and the stability of the cavity, this is limited. Making the incoupled beam smaller which, as already mentioned, makes the focus larger, yields more power in the cavity but the highest cavity power appears still at the edge of stability, see Fig. 3.2. So an even smaller beam is generated with a different lens setup, resulting in even more incoupled intensity (black curve). As shown, there is

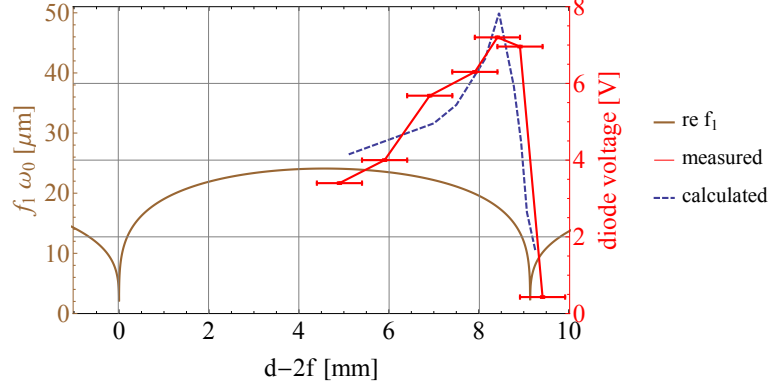


Figure 3.3: Measured intra-cavity power and the calculated mode matching, (which is scaled to the measured power). The calculated mode matching and the measured cavity power maximum are nearly at the same position.

a power maximum. Making the beam even smaller just shifts the best mode matching position too larger focus size which is counterproductive for high harmonic generation. Note that this measurement is made with a precision of half a millimeter of the cavity mirror distance, and also with a step size of one millimetre. As a result the maximum of the power may not be captured. Also the intra-cavity power depends on several parameters like alignment, cleanliness of the cavity mirrors and power of the incoming light. However, this measurement serves as a good starting point for the calculation to get an exact mode matching. Considering the measured beam parameter of the laser source and the setup one can generate a model by building the ABCD-matrix for the incoming beam:

$$\begin{pmatrix} A & B \\ C & D \end{pmatrix} = \begin{pmatrix} 1 & d/2 \\ 0 & 1 \end{pmatrix} \begin{pmatrix} 1 & 0 \\ -2\cos(\theta)/R & 1 \end{pmatrix} \begin{pmatrix} 1 & l_{f1} + \delta l_{lens1} \\ 0 & 1 \end{pmatrix} \begin{pmatrix} 1 & 0 \\ -1/f_{lens1} & 1 \end{pmatrix} \begin{pmatrix} 1 & l_{bc} - \delta l_{lens1} - \delta l_{lens2} \\ 0 & 1 \end{pmatrix} \begin{pmatrix} 1 & 0 \\ -1/f_{lens2} & 1 \end{pmatrix} \begin{pmatrix} 1 & \delta l_{lens2} + l_0 \\ 1 & 1 \end{pmatrix}. \quad (3.1)$$

This model can be compared to the empirically found configuration, the mode matching for a focused beam diameter ω_{foc} and the cavity diameter ω_c . The mode matching is just calculated as a factor of ω_{foc} and ω_c :

$$\begin{aligned} m_m &= \omega_c / \omega_{foc} & \omega_c < \omega_{foc}, \\ m_m &= \omega_{foc} / \omega_c & \omega_c > \omega_{foc}. \end{aligned} \quad (3.2)$$

Figure 3.3 shows the measured intra-cavity power for the used setup, and the calculated mode matching which is scaled to the measured power. It can be seen that the measurement shows the ideal mode matching nearly at the measured maximum. Fine tuning the position of the lens shifts the position of the mode matching to the size of the preferred intra-cavity focus.

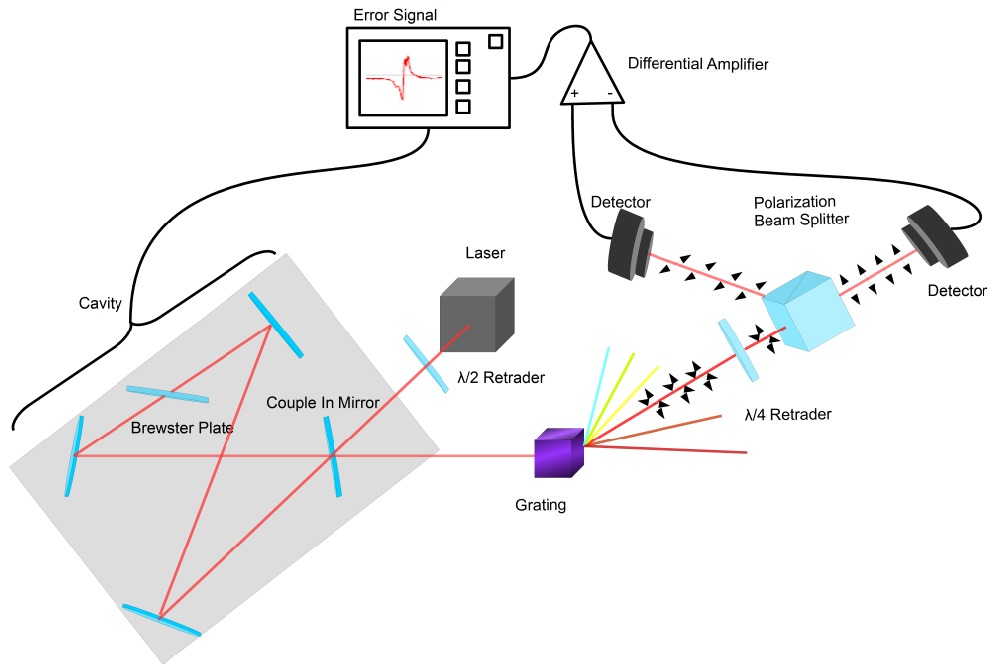


Figure 3.4: Hänsch and Couillaud setup for stabilization of an enhancement cavity on resonance. In the cavity there is a Brewster plate which serves as linear polarizer, the $\lambda/2$ -wave plate in front of the cavity controls the polarization of the incoming light. The strength of the error signal depends on the angle θ between the polarization of the incoming light and the polarization axis of the Brewster plate. But θ also changes the intensity of the in-coupled light. Note that sometimes small changes of θ may change the quality of the error signal dramatically but do not influence the intra-cavity power much. Thus, it is always worth a try to fine tune this angle. The reflected beam is sent to a grating to split it up in the spectral parts. A quarter-wave plate with the fast axis parallel to the polarization axis of the cavity, and polarization beam splitter and two photodiodes are used to analyze the polarization of the reflected beam.

3.2 T.W. Hänsch and B. Couillaud Stabilization

To match the length of the enhancement cavity to the repetition frequency of the frequency comb, the stabilization method invented by T.W. Hänsch und B. Couillaud is used [18]. The advantage of this technique is that there is no need for modulation techniques and if there are any large jumps in the cavity length caused by vibrations or thermal fluctuations, the error signal should be strong enough to relock the cavity even if it is far away from the resonance [18]. The setup can be seen in Fig. 3.4.

The $\lambda/2$ -wave plate in front of the cavity in combination with a Brewster plate is used to control the power and also to set an angle θ between the polarization of the incoming light and the polarization axis of the Brewster plate which serves as a linear polarizer. The light coupled into the cavity consists of two linear polarized components. One of them parallel to, the other one perpendicular to the transmission axis of the Brewster plate. If one approximates the incoming light as a plane wave, the field amplitudes parallel $E_{\parallel}^{(i)}$ and perpendicular $E_{\perp}^{(i)}$ to the polarization axis are given by

$$\begin{aligned} E_{\parallel}^{(i)} &= E^{(i)} \cos(\theta), \\ E_{\perp}^{(i)} &= E^{(i)} \sin(\theta), \end{aligned} \quad (3.3)$$

where $E^{(i)}$ is the amplitude of the incident beam. Due to the filtering of the Brewster plate the different fields $E_{\parallel}^{(i)}$ and $E_{\perp}^{(i)}$ of the laser see different cavities. For $E_{\parallel}^{(i)}$ the Brewster plate generates quite low losses (if it exactly equals the Brewster angle). For $E_{\perp}^{(i)}$ the cavity is an absorber. To calculate the amplitude of the reflected beam $E^{(r)}$, which consists of two different parts: a cavity with an in-coupling-mirror, with a reflectivity coefficient r_m and transmission coefficient t_m and the rest of the cavity with a wave reflectivity coefficient for one round trip r_c , which accounts for any losses in the cavity. The calculation of the electric field which is reflected by the cavity resembles the calculation for the intensity which builds up in the cavity, see Sec. 2.1. The beam which is reflected at the in-coupling-mirror, is superposed with the beams which are transmitted from the cavity through the in-coupling-mirror after the cavity round trips. The electric field reflected from the cavity for the first three cavity round trips is given by,

$$E_{\parallel}^r(1) = r_m E_{\parallel}^{(i)}, \quad (3.4)$$

$$E_{\parallel}^r(2) = t_m t'_m r_c E_{\parallel}^{(i)} e^{i\varphi}, \quad (3.5)$$

$$E_{\parallel}^r(3) = t_m t'_m r_c r'_m r_c E_{\parallel}^{(i)} e^{2i\varphi}, \quad (3.6)$$

$$E_{\parallel}^r(4) = t_m t'_m r_c r'_m r_c r'_m r_c E_{\parallel}^{(i)} e^{3i\varphi}. \quad (3.7)$$

$$(3.8)$$

Therefore, the complete reflected parallel electric field for infinite round trips is given by:

$$E_{\parallel}^r = \left(r_m + t_m t'_m r_c e^{i\varphi} \sum_{n=0}^{\infty} (r_c r'_m e^{i\varphi})^n \right) E_{\parallel}^{(i)}. \quad (3.9)$$

Once again, with $r_c r'_m e^{i\varphi} < 1$ and using the geometric series one gets the reflected parallel electric field component:

$$E_{\parallel}^r = \left(r_m + \frac{t_m t'_m r_c e^{i\varphi}}{1 - r_c r'_m e^{i\varphi}} \right) E_{\parallel}^{(i)}. \quad (3.10)$$

Using

$$r_m = -r_m, \quad (3.11)$$

$$R_m = r_m^2, \quad (3.12)$$

$$R_c = r_c^2, \quad (3.13)$$

$$T_m = t_m t'_m, \quad (3.14)$$

one can write $E_{\parallel}^{(r)}$ as,

$$E_{\parallel}^{(r)} = E_{\parallel}^{(i)} \left(\sqrt{R_m} - \frac{T_m}{\sqrt{R_m}} \frac{\sqrt{R_m R_c} e^{i\varphi}}{(1 - \sqrt{R_m R_c} e^{i\varphi})} \right), \quad (3.15)$$

$$\Rightarrow E_{\parallel}^{(r)} = E_{\parallel}^{(i)} \left(\sqrt{R_m} - \frac{T_m \sqrt{R_m R_c}}{\sqrt{R_m}} \frac{\cos \varphi - \sqrt{R_m R_c} + i \sin \varphi}{(1 - \sqrt{R_m R_c})^2 + 4\sqrt{R_m R_c} \sin^2 \frac{1}{2}\varphi} \right). \quad (3.16)$$

$\sqrt{R_m R_c}$ accounts for the attenuation of every cavity round trip, including the reflections by the cavity mirrors, the losses caused by the out-coupler, the polarizer, and the high harmonic generation losses. For the perpendicular component $\sqrt{R_m R_c}$ can be set to zero due to the large losses in the cavity and it follows:

$$E_{\perp}^{(r)} = E_{\perp}^{(i)} \sqrt{R_m}. \quad (3.17)$$

If the cavity is on resonance which means $\varphi = 2n\pi$, E_{\parallel} becomes

$$E_{\parallel}^{(r)} = E_{\parallel}^{(i)} \left(\sqrt{R_m} - \frac{T_m \sqrt{R_m R_c}}{\sqrt{R_m}} \frac{-\sqrt{R_m R_c}}{(1 - \sqrt{R_m R_c})^2} \right). \quad (3.18)$$

As it can be seen, $E_{\parallel}^{(r)}$ on resonance is a real function which means there is no phase shift between the two reflected components, and the reflected beam remains linearly polarized. If the cavity is not on resonance the imaginary part of $E_{\parallel}^{(r)}$ is not zero and the parallel and the perpendicular beam are not in phase. Hence, the reflected beam is elliptically polarized. The important thing is that the handedness of this polarization ellipse is different for the two sides of the resonance. Thus, by analyzing the polarization one can say on which side of the resonance the cavity length is. This can be used to stabilize the cavity on resonance. The setup which is needed for analyzing the polarization can be seen in Fig. 3.4. Since it is not a cw-laser but a pulsed femtosecond laser one cannot use this light directly, but instead has to split it up with a grating. After the grating there is a quarter wave plate which transforms the elliptically polarized light to linearly polarized light again. Behind the wave plate a polarization beam splitter splits up the orthogonal and perpendicular components which are analyzed by two photodiodes. To fine-tune the signal one of these photodiodes is connected to an amplifier which also can add an offset to the signal. After this amplifier there is a differential amplifier which generates the final error signal. Depending on the stability of the cavity and the speed of the amplifying electronics it is beneficial to use a low-pass filter to cut away the very fast length changes which may ask too much of the stabilization electronic. This sometimes helps to make the lock more stable. If the fast axis of the quarter wave plate is parallel to the polarization axis of the cavity the amplitude of the electric field after the wave plate and the beam-splitter is given by:

$$E_{a,b} = \frac{1}{2} \begin{pmatrix} 1 & \pm 1 \\ \pm 1 & 1 \end{pmatrix} \begin{pmatrix} 1 & 0 \\ 0 & i \end{pmatrix} \begin{pmatrix} E_{\parallel}^{(r)} \\ E_{\perp}^{(r)} \end{pmatrix}. \quad (3.19)$$

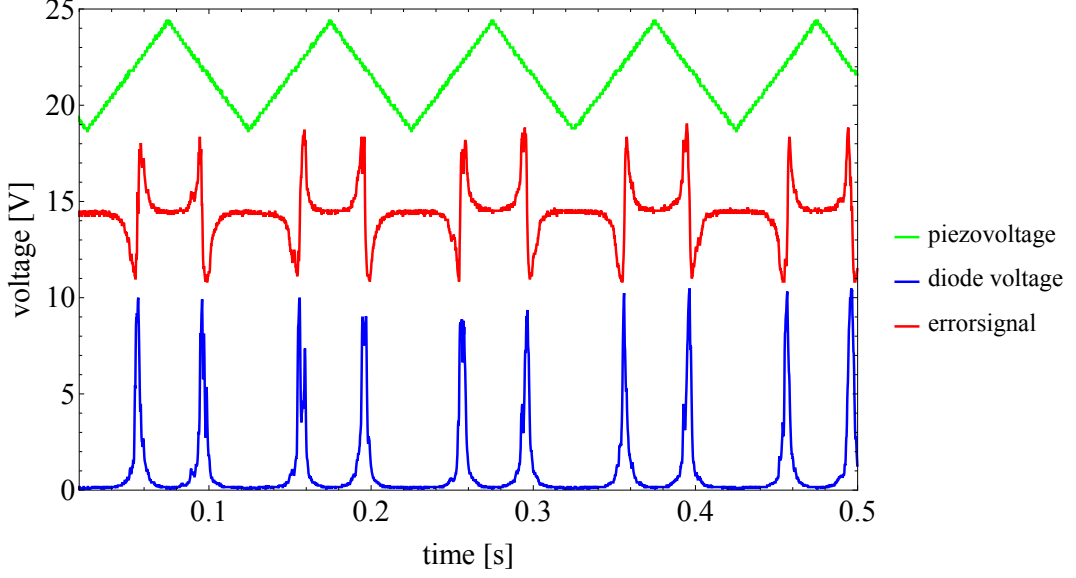


Figure 3.5: Cavity length modulation by a Piezo which is glued to a cavity mirror. The green dashed line shows the voltage which is applied to the Piezo. The Blue dotted line represents the intra-cavity power measured by a photodiode. The Piezo scans over the resonance. The red line shows the error signal generated from the Hänsch-Couillaud-stabilization-setup.

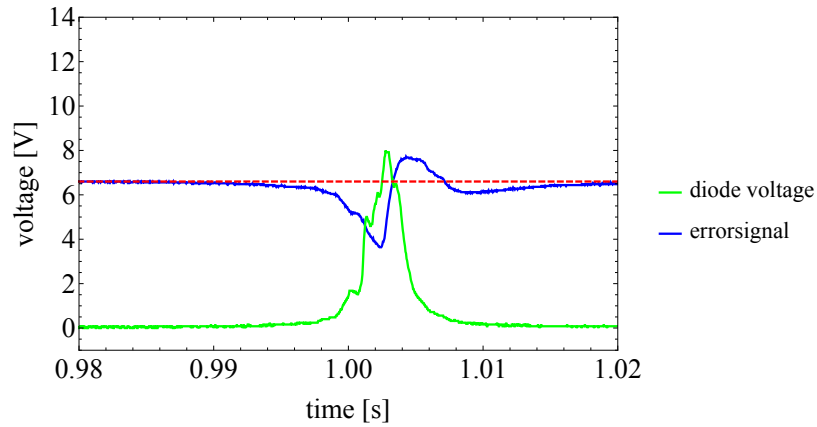
The intensity which is measured by the photodiodes is therefore given by:

$$I_{a,b} = \frac{1}{2} c \epsilon |E_{a,b}|^2 = \frac{1}{2} c \epsilon \left| \frac{1}{2} E_{\parallel}^{(r)} \pm E_{\perp}^{(r)} \right|^2. \quad (3.20)$$

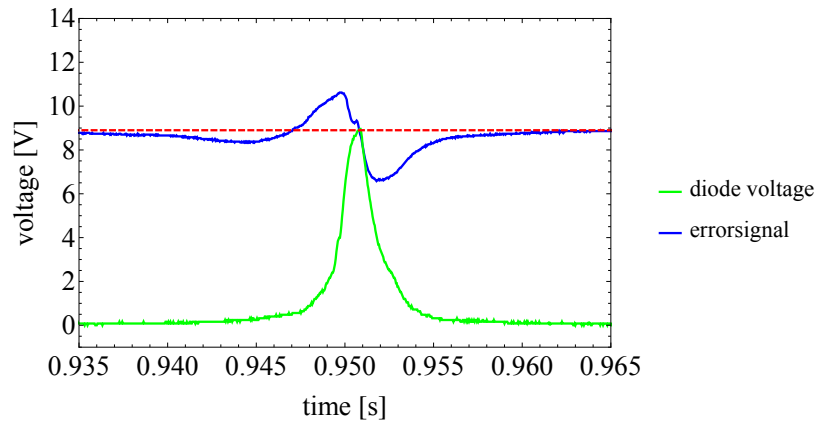
This leads to an error signal which is generated by the differential amplifier:

$$I_a - I_b = c \epsilon \left| E^{(i)} \right|^2 \cos \theta \sin \theta \frac{T_m \sqrt{R_m R_c} \sin \varphi}{(1 - R)^2 4 \sqrt{R_m R_c} \sin^2 \frac{1}{2} \varphi}. \quad (3.21)$$

Figure 3.5 shows a scan over the resonance curve of the cavity. The green dashed line represents the voltage of a Piezo which is glued to a cavity mirror. The Piezo is driven by a triangular voltage coming from a frequency generator which is amplified by a high voltage amplifier. With a stepmotor one can set the cavity length roughly close to resonance and afterwards the Piezo scans over the resonance. The blue dotted line shows the cavity power, the red one the corresponding error signal. However, just one of the infinite comb modes is stabilized to one of the infinite cavity modes. Depending on which spectral part of the light is sent from the grating to the error signal setup different comb modes can be stabilized. Dispersion in the cavity leads to a unexpected behaviour of the error signal. The dispersion shifts the cavity modes from mode to mode, as it can be seen in Fig. 2.8. This means the stabilization of any cavity mode to any comb mode can result in quite different intra-cavity powers, see Fig. 3.6(a). Instead of locking the cavity to the maximal possible intensity the error signal is shifted and therefore



(a)



(b)

Figure 3.6: Shifted error signal (a), the locking position of the error signal does not lock the cavity length to the maximum of the possible intra-cavity power; non shifted error signal (b), the cavity length can be locked to the maximum of possible intra-cavity power.

stabilizes the cavity to some lower intensity. If we only consider linear dispersion in the cavity this problem can be eliminated by using two Hänsch and Couillaud setups, at two different cavity modes. One for stabilizing the cavity length and one for stabilizing the comb offset. This dual stabilization suppresses any degrees of freedom for the comb and the cavity modes. Hence, they should be matching exactly. Higher order dispersion can again yield a shifted error-signal.

4 Implementation

4.1 Optical Setup Overview

The whole setup is shown in Fig. 4.1. The frequency comb-1 is mounted on a floating optical table-2. The 3D-cavity setup is located in a vacuum chamber-3, which is mounted on a breadboard-4, to get the correct height to be matched to the spectrograph, and also to have another vibration damping element between the table surface and the chamber. The beam of the frequency comb can be pre-compressed by a prism compressor-6 or a chirped mirror beam pass. This has to be done because the beam travels outside the vacuum chamber through air, through the focusing lenses, through a glass plate of the vacuum chamber and finally through the in-coupling-mirror, all of which spectrally broaden the pulse. The beam is lifted to the level of the cavity, as close as possible to the in-coupling-mirror of the cavity. The beam pass from the comb to the cavity is as close as possible to the optical table to minimize vibrations. To send the beam into the cavity the beam has to be lifted as already mentioned. Therefore vibration damping components are used 7. The reflected beam is sent to a T.W. Hänsch and B. Couillaud stabilization setup, to stabilize the cavity on resonance as described in Sec. 3.2.

4.2 Planar Ring-Cavity Setup

During this master thesis two different cavity types are used. In order not to change the 3D-cavity setup, a planar ring cavity is built and used for stability testing. Figure 4.2 shows the ring cavity. For a better overview, the numberings of the different components are colour coded. Cavity mirrors are blue, Piezo length changing and alignment elements are red, focus positions are green, and the rest of the optic is magenta. To achieve a more compact setup six mirrors are used. The light is coupled in through the in-coupling-mirror $M1$, the beam travels from mirror $M1$ to mirror $M2$. The transmitted beam of mirror $M2$ is sent too a mirror $O1$ and from there to a pellicle beamsplitter $O2$, (for data sheet see A.7¹). The beam transmitted through the pellicle is sent to a photodiode $O4$, (for data sheet see A.9) and the beam reflected from the pellicle is sent to a CCD-camera $O5$ ². The CCD-camera ideally is placed exactly at the same distance from mirror $M2$ as the focus f_2 so the focus is imaged onto the camera. This is very useful for positioning a focusing lens in front of the the cavity. From mirror $M2$ the beam travels to the first curved cavity mirror $M3$. The second focus of the cavity is located somewhere along this beam path. The angle of incidence should be as small as possible to make the stability shift between the horizontal and the vertical focus as

¹The A numbers can be found in the annex.

²Logitech HD Webcam C270.

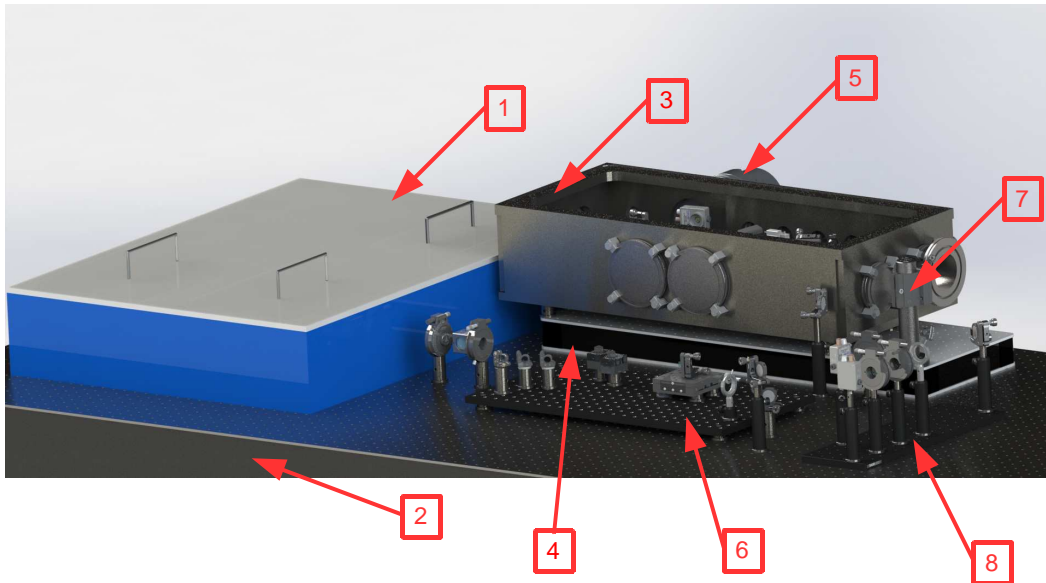


Figure 4.1: The complete setup on the optical table: Frequency comb-1, floating optical table-2, vacuum chamber-3, breadboard-4, turbo molecular vacuum pump-5, prism compressor-6, vibration damping in-coupling setup-7, T.W. Hänsch and B. Couillaud stabilization setup-8. A detailed description of the parts can be found in the annex A.

small as possible, see Sec. 2.3. Between mirror $M3$ and $M4$ the beam is focused at f_1 . Mirror $M4$ is mounted on a translation stage $P2$, (for data sheet see A.8) to change the distance of the curved cavity mirror to vary the focus size of the cavity eigenmode. From $M4$ the beam travels to mirror $M5$, the emergent angle has to have the same size as the angle of incidence between mirror $M2$ and $M3$, otherwise a shift would occur in the stability ranges. Mirror $M5$ is mounted in a Piezo-motor-driven-optical-mount, (for data sheet see A.10), to align the cavity. Also mirror $M1$ is mounted to Piezo-motor-driven-optical-mount. Mirror $M5$ is also mounted on a translation stage $P4$ to change the cavity length to go on/off resonance or to compensate the length change of the other stage. From mirror $M5$ the beam travels to mirror $M6$, this mirror is glued to a Piezo $P3$ to fine tune the cavity length, scan over the resonance and to stabilize the cavity on resonance. Finally the beam travels from mirror $M6$ to mirror $M1$ and the cavity round trip is finished.

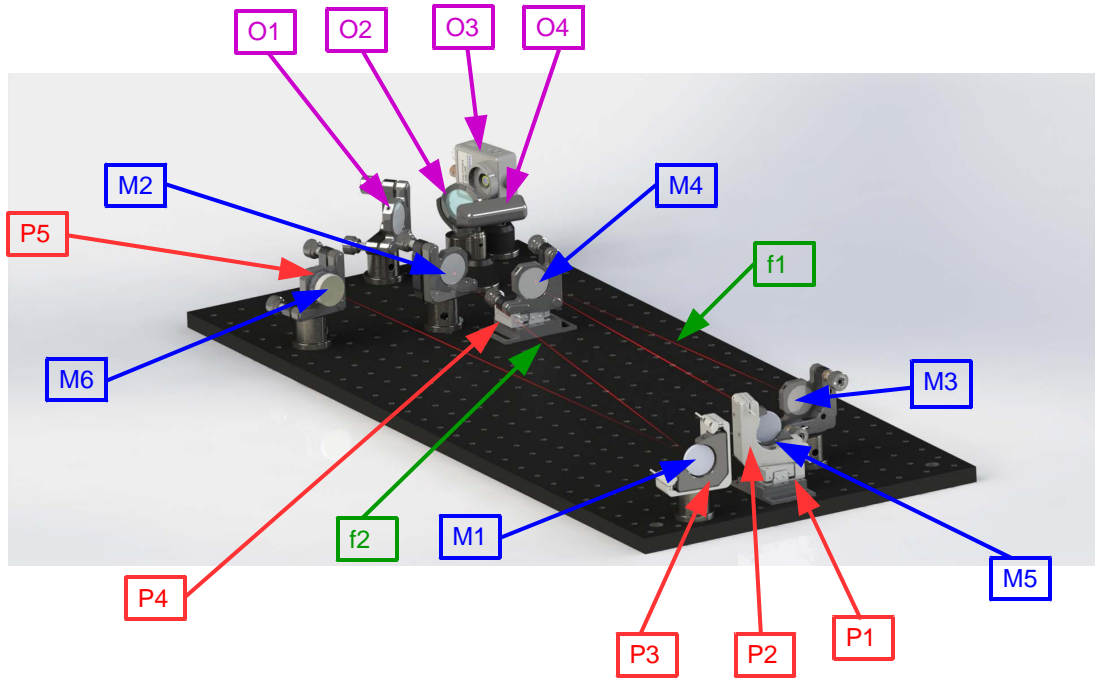


Figure 4.2: Structure of the ring cavity setup. Cavity length 2.771 m, M1-in-coupling-mirror, M2-M5-M6-High reflector mirrors, M3-M4 curved cavity mirrors $R=150$ mm, P1-P4-Piezo motor-driven-linear-stage, P2-P3-Piezo-motor-driven-optical-mount, f_1 -position of primary cavity focus, f_2 -position of secondary cavity focus, P5-Piezo, O1-silver mirror, O2-pellicle beamsplitter, O3-photodiode, O4-CCD-Camera.

4.3 3D-Cavity Setup

The second setup which is used is the 3D-setup as it was introduced in Sec. 2.3. Figure 4.3 shows the 3D-cavity setup which is a little bit more complex. Again the numbering of the different components are colour coded. Cavity mirrors are blue, Piezo length changing and alignment elements are red, focus positions are green, high harmonic generation components yellow, and the rest is magenta. The light is coupled-in through the in-coupling-mirror M_1 , which is mounted to Piezo-motor-driven-optical-mount. The beam travels from mirror M_1 to mirror M_2 . The transmitted beam of mirror M_2 is sent over a mirror O_1 to a pellicle beamsplitter O_2 , (for data sheet see A.7). The beam transmitted through the pellicle is sent to a photodiode O_4 , (for data sheet see A.9), and the beam reflected from the pellicle is sent to a CCD-camera O_5 . Ideally the CCD-camera is placed exactly at the same distance from mirror M_2 as the focus f_2 so the focus is imaged onto the camera. This is very useful for positioning a focusing lens in front of the the cavity. Mirror M_2 shifts the beam just vertically and sends it to mirror M_3 , the second focus of the cavity can be found somewhere along this beam

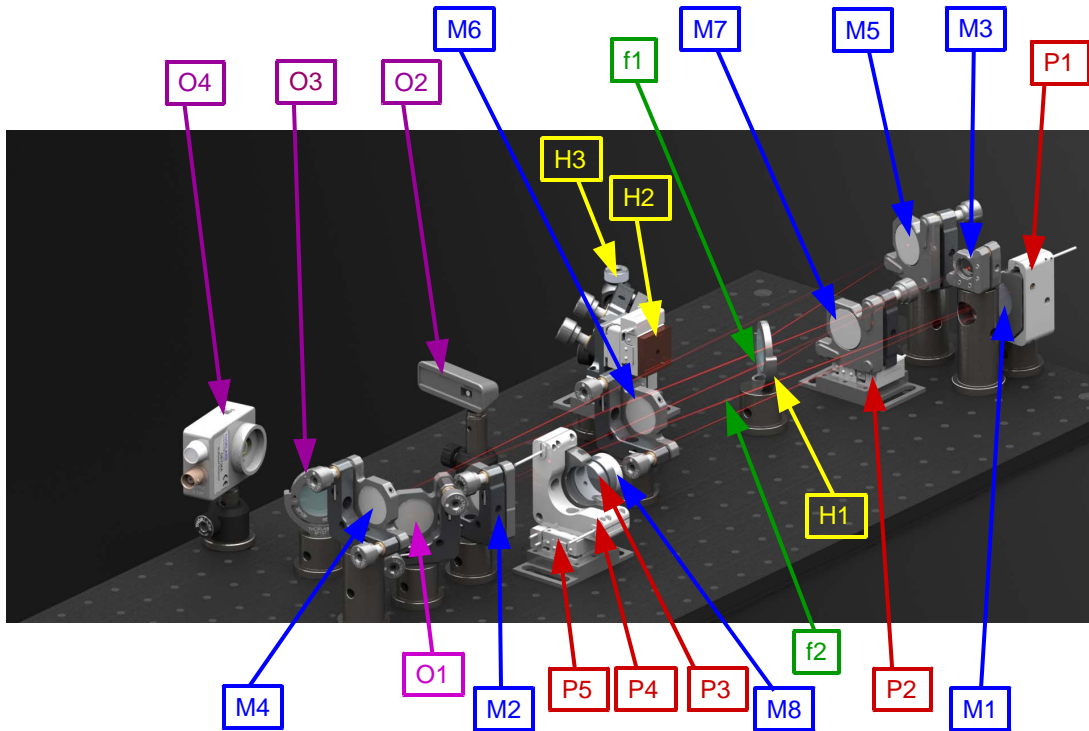


Figure 4.3: Structure of the 3D-cavity setup. Cavity length 2.771 m, M1-in-coupling-mirror, M2-M3-M4-M5-M8-high reflector mirror, M6-M7 curved cavity mirror $R=150$ mm, P2-P5-Piezo motor-driven-linear-stage, P4-P1-Piezo-motor-driven-optical-mount, f1-position primary cavity focus, f2-position secondary cavity focus, P3-Piezo, O1-silver mirror, O2-CCD-camera Logitech HD webcam C270, O3-pellicle beamsplitter A.7, O4-photodiode, H1-out-coupler, H2-Xenon jet, H3-out-coupling-mirror.

path. Mirror $M3$ shifts the beam horizontally and sends it to Mirror $M4$. Again the beam is just shifted horizontally and sent to Mirror $M5$. Mirror $M5$ shifts the beam vertically and sends it to the first curved cavity mirror $M6$. This angle of incidence should be as small as possible to gain just a small shift between the horizontal and the vertical foci, see Sec. 2.3. From mirror $M6$ the beam travels to the second curved cavity mirror $M7$, the focus f_1 is located at this path. Mirror $M7$ shifts the beam horizontally and sends it to Mirror $M8$. This emergent angle in the horizontal plane has to be the same as the angle of incidence between mirror $M5$ and $M6$ in the vertical plane. Mirror $M8$ is mounted on a translation stage $P5$, a Piezo is glued to this mirror and it is also on a Piezo-motor-driven-optical-mount $P4$. From mirror $M8$ the beam is sent to mirror $M1$ and the cavity round trip is finished.

4.4 Aligning a Ring-Cavity

If one builds a ring- or a 3D-cavity and wants to align it, it may not seem to be an easy task. The first alignment which was done during this master thesis took quite a while, while, whereas the last one only a few minutes. The most important alignment tool is a simple webcam with removed infrared filter. The infrared filter is a thin, brittle glass plate, close to the camera chip, which has to be removed. During the removal it is important not to break the filter, this would destroy the camera. A good way to remove the filter is to pile glue on the filter and after curing pull the glue off with a gripper. The filter should come off with it. A difficult job is to find the right position for the camera, because the light which transmits through the high reflector mirrors is very weak. One can hardly observe it, even with an infrared viewer. A good approach is to put the camera straight behind the high reflector mirror, catch the beam there and slowly move the camera to the position it should be. Normally there is another mirror and also a pellicle beamsplitter in the beam path to the camera. However, by a fortunate coincidence the frequency comb used in this master thesis also has a spectral part in the infrared range. If this part is not filtered out by a prism compressor or filter, it nearly fully transmits through the high reflector mirrors and can be used to align the camera, afterwards it has to be filtered out. If the camera is at the correct position, the next step is to align the first round of the cavity. It is critical to hit the cavity mirrors in the middle. Next step is to find the reflection of the in-couple mirror and send it to the second cavity mirror. It should be possible to see the reflection of the first cavity mirror with a piece of paper somewhere on the second cavity mirror. With the help of the Piezo-optical-mirror-mount it is possible to iteratively overlay the beam on the first and second cavity mirror until the second beam appears on the camera. This is done by changing the horizontal and/or vertical direction of one of the mirrors to align the beam at the first cavity mirror, and changing the horizontal or/and vertical direction of the second mirror to align the beam at the second cavity mirror. Usually two beams are enough to align the cavity, by just choosing a high enough speed of the Piezo mounts and randomly try the different directions until a third beam appears on the camera. With three beams on the camera it is straight-forward to align the beams until more and more beams appear on the camera and finally the cavity is aligned, this can schematically be seen in Fig. 4.4.

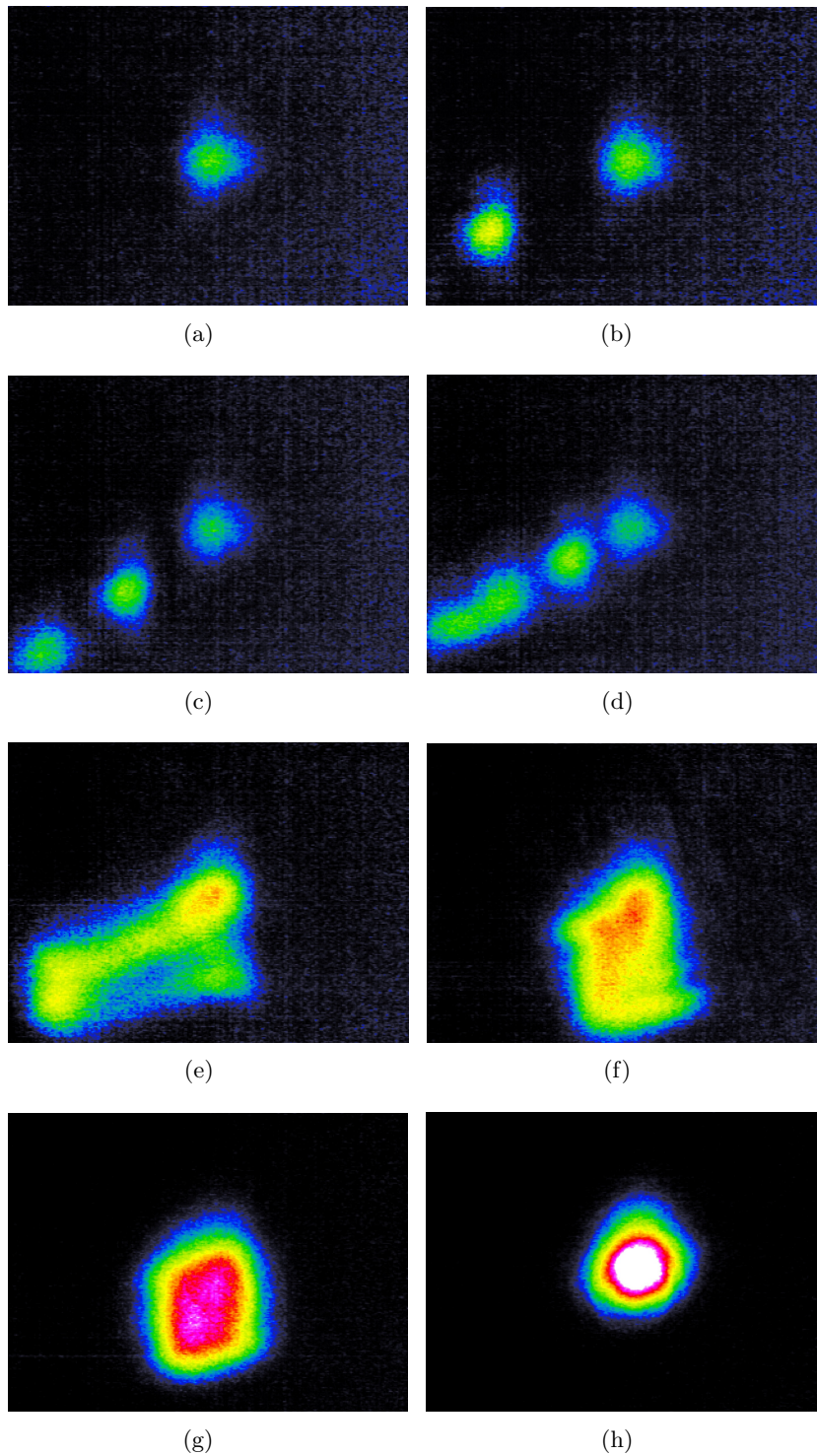


Figure 4.4: View on the ccd camera during the alignment. In-coupled beam (a), first round trip of cavity aligned (b), second round trip of cavity aligned (c), and so on (d), (e), (f), (g). Aligned cavity (h).

4.5 Hänsch Couillaud Stabilization Setup

The implementation of the Hänsch Couillaud error signal is quite straight-forward. Figure 4.5 shows the setup with the used components. The grating-1, splits the beam into its spectral components and sends it through an iris-2, which blocks all unnecessary beam parts. A quarter wave-plate-3, and a polariser beam splitter cube-4, analyze the beam and two photodiodes-5,-6, measure the intensity of the different beam parts.

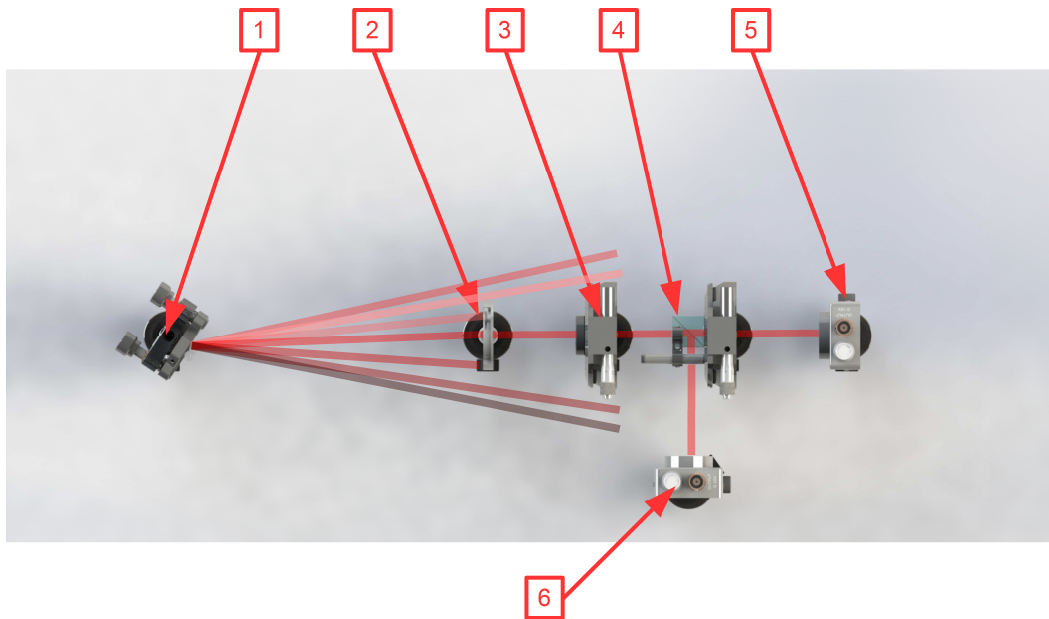


Figure 4.5: Implementation of the Hänsch-Couillaud-error-signal, 1-Grating, 2-Iris, 3- $\lambda/4$ -Wave plate, 4-Polarisation beam splitter cube, 5-6-Photodiode.

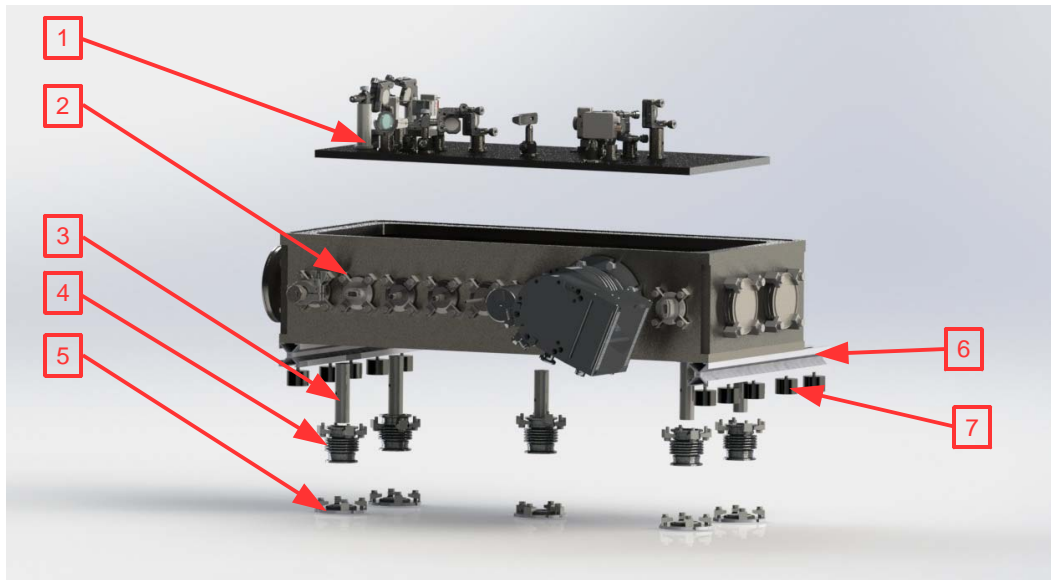
4.6 Connection of the Cavity and the Optical Table

Figures 4.6(a) and 4.6(b) show how the cavity is connected with the optical table. The main goal of the complete setup is to keep the cavity isolated from vibrations, therefore a lot of time and effort were invested. The vibration damping was implemented by fixing the cavity-1, to five one inch posts-3, which are fixed to an aluminium plate-5, which in turn is fixed to the optical table. The posts are fed into execution holes in the vacuum chamber-2. Everything is sealed with flexible vibration damping vacuum tubes-4. The chamber is mounted on two item bars-7, to get the correct height and stands unmounted on several vibration damping rubber feet-6, this leads to the cavity and the vacuum chamber not being connected. Tests showed that this design really isolated

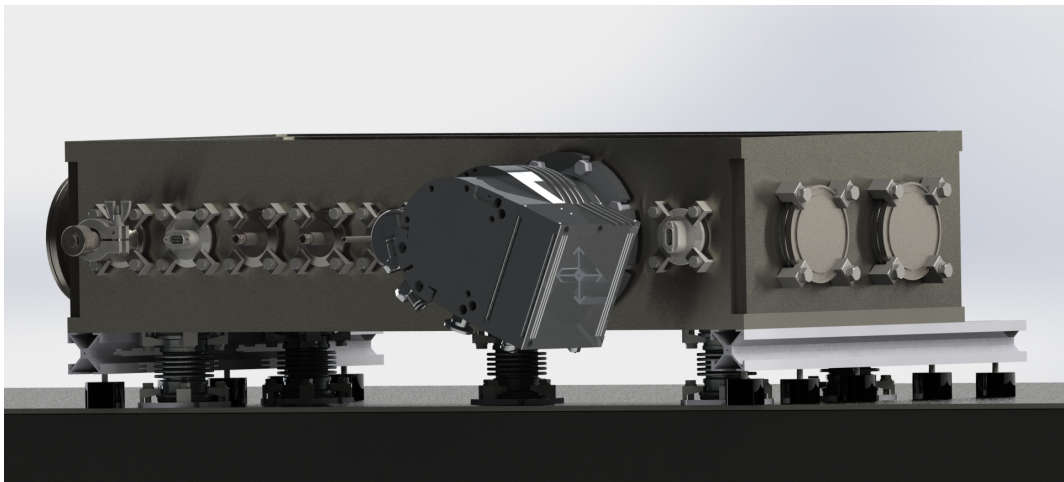
the optics from vacuum pump vibrations, but it does not manage to keep the cavity isolated from other vibrations. The intra-cavity power on resonance is fluctuating nearly by 100 %, three times every 10 ms, see Fig. 4.7(a). The signal was Fourier analysed and it showed two significant peaks. One at 300 Hz and one at 600 Hz, see Fig. 4.7(b). Tests with a loudspeaker and a sound generator showed that the peak at 300 Hz could be enhanced by playing sounds in the laboratory close to the 300 Hz. Figure 4.7(c) shows the distribution of the cavity power on resonance. A normal distribution

$$g(x) = \frac{A}{\sigma\sqrt{2\pi}} e^{-\frac{1}{2}\left(\frac{x-\mu}{\sigma}\right)^2}, \quad (4.1)$$

was fitted, where A is an amplitude, σ is the standard derivation and μ is the mean of the derivation. The fitted Gauss function has a mean enhancement of 27 and a standard derivation of 40. However, due to the periodic fluctuation the Gauss function is not a good approximation for these measuring data. The fluctuation could be measured even if the cavity was in vacuum, so it seems as if the vibrations come from the air, are collected by the optical table and transferred and magnified by the posts on which the cavity is mounted. This is not surprising if one takes a closer look at the spec-sheet of the optical table, see Fig. 4.8. The vibration damping of the table works well for lower frequencies below 50 Hz, but not for higher frequencies. A measurement series with an acceleration sensor reveals the truth: On the optical table, on the cavity breadboard and on the cavity mirrors, a vibration with a frequency of 360 Hz could be measured as it can be seen in Fig. 4.9. Note the perturbation frequency changed for different optical table configurations. There seemed to be a resonance frequency which depends on the weight distribution on the optical table and the cavity position. To isolate the cavity from the vibration of the optical table the complete setup was reconstructed.

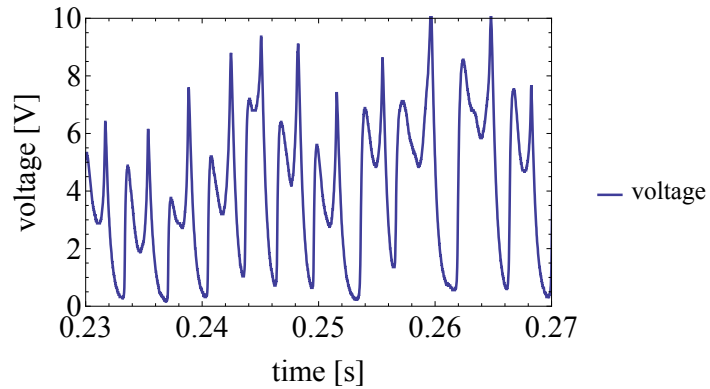


(a)

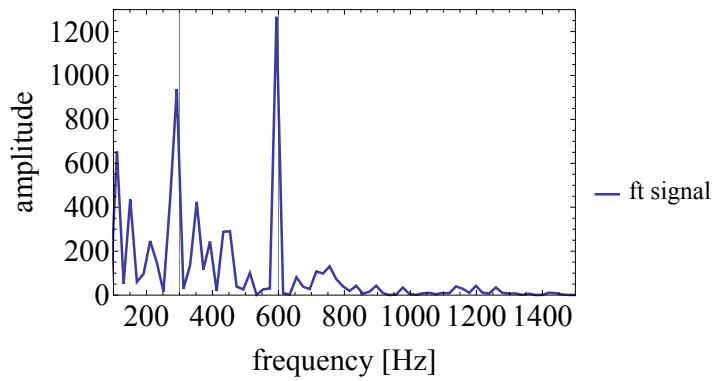


(b)

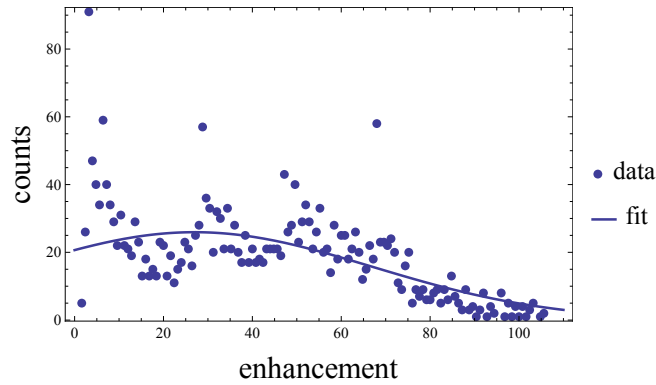
Figure 4.6: Design of the connection of the cavity, the vacuum chamber and the optical table. Exploded view (a), composite configuration (b).



(a)



(b)



(c)

Figure 4.7: Cavity on resonance with an enhancement of 100, diode signal (a), Fourier analysis of the diode signal 4.7(b), distribution of the enhancement 4.7(c). Without any modulation, nearly a 100% fluctuation of the power three times every 10 ms can be observed. This means, that a perturbation of the cavity with 300 Hz brings the cavity off and on resonance.

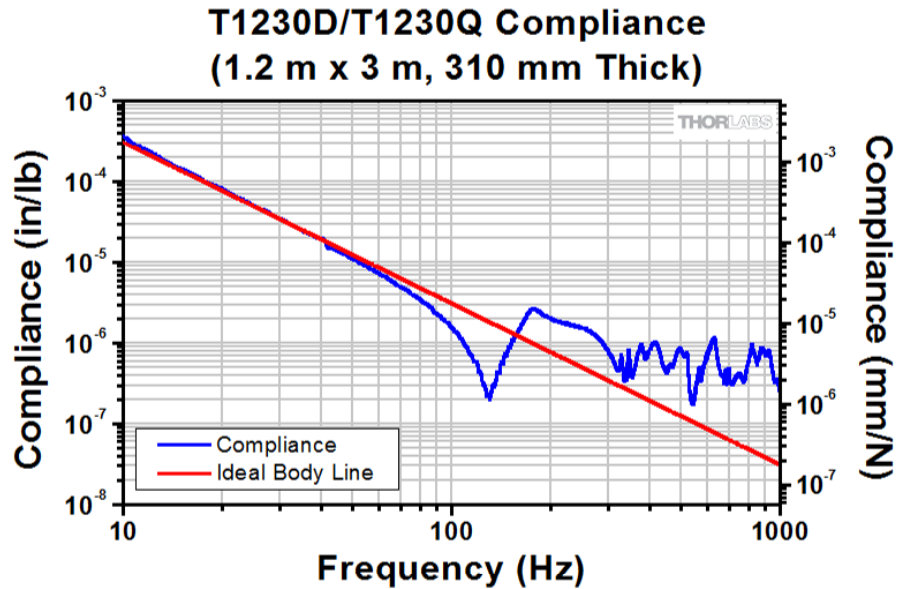


Figure 4.8: Data sheet of the optical table. It can be seen that the vibration damping of the table works well for lower frequencies below 50 Hz, but not for higher frequencies.

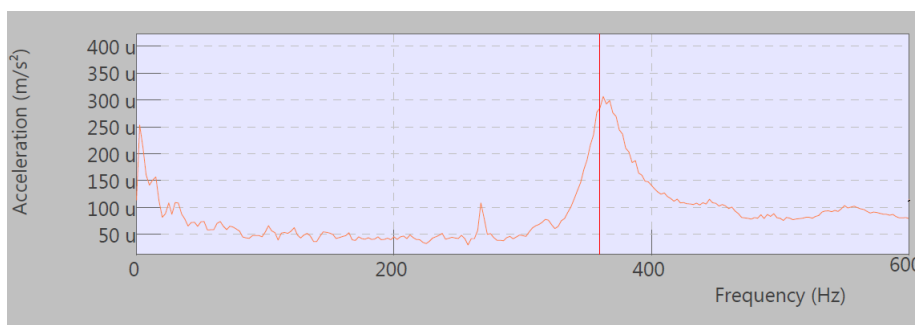
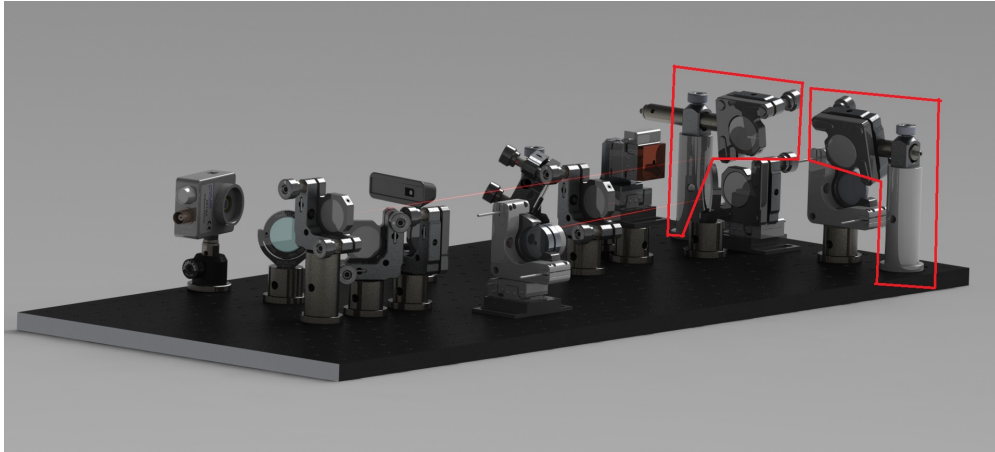
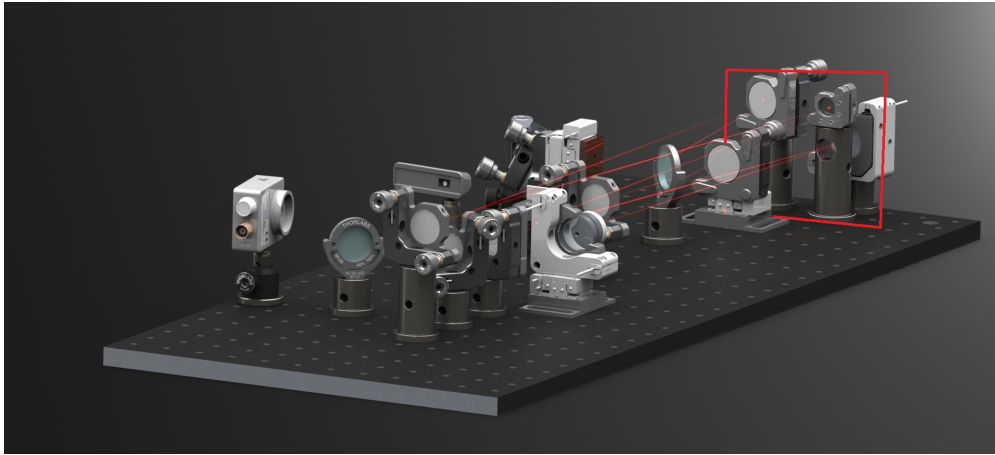


Figure 4.9: Measurement with an acceleration sensor, which was fixed to the breadboard of the cavity, it showed a small peak at 360 Hz after knocking to the optical table with a screwdriver, the peak increases.



(a)



(b)

Figure 4.10: Rebuilding the 3D-cavity by solving the polarization conditioned design problem with a special post. The old setup (a); the improved cavity design (b).

4.7 Reconditioning the 3D-Cavity

The first attempt to improve the stability of the cavity was to rebuild the cavity itself, as it can be seen in Fig. 4.10. To eliminate the problem of a polarisation twist during the cavity round trip, the beam was just moved either horizontally or vertically, but not at the same time. This made it necessary to place mirrors at the same X-Y position on the breadboard but at different heights. This was implemented with an unsuitable construction, see Fig. 4.10(a). The design problem was solved by drilling a hole into a post, which was large enough not to influence the enhancement but small enough not to influence the stability of the post. The new setup can be seen in Fig. 4.10(b). These changes should make the cavity more stable but the vibrations which came from the optical table were still too strong to see an improvement in the stability. The next step

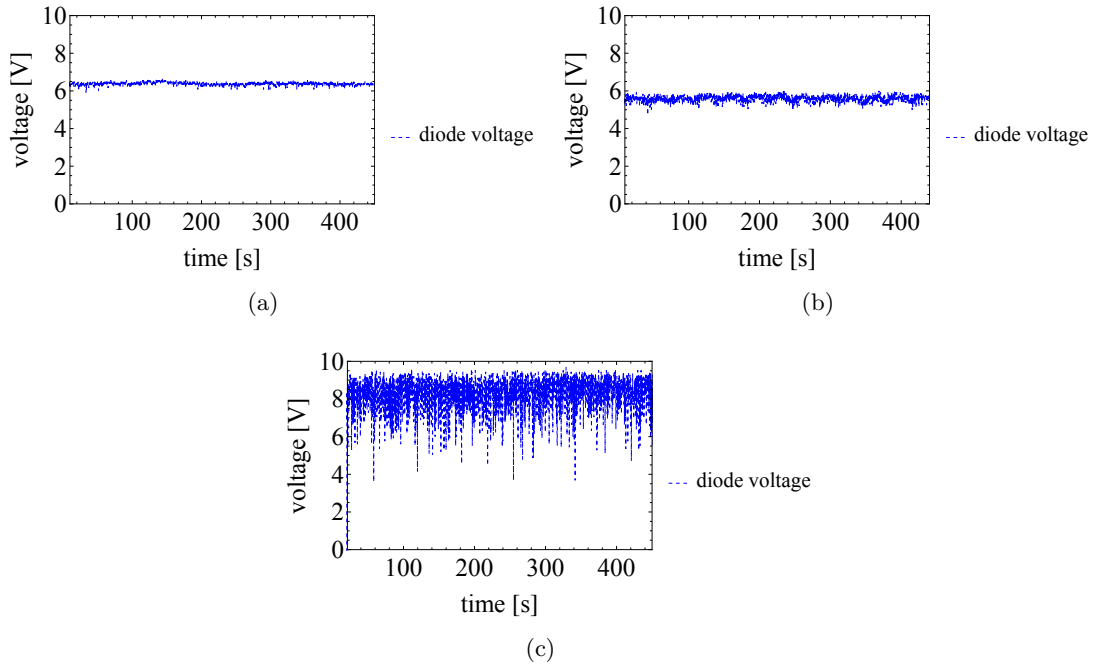


Figure 4.11: Stability of the planar ring cavity setup for different enhancements. Lock with an enhancement of 30 (a), lock with an enhancement of 45 (b), lock with an enhancement of 85 (c).

was to build a more stable setup with the given components. With the ring cavity setup as it was described in Sec. 4.2, many different possibilities were tested. Particular attention was paid to measuring the stability of the different setups with nearly the same enhancement. The enhancement influences the stability dramatically, as it can be seen in Fig. 4.11. For a cavity with high enhancement the cavity mode peak is quite narrow and for lower enhancement the peak becomes much broader, as shown in Fig. 4.12. For smaller enhancement the matching of the comb modes to the cavity modes is not that sensitive to perturbation, which shifts the cavity modes, and the cavity appears more stable compared to a cavity with high enhancement. The stability measurements were made with an enhancement between 40 and 60. First change on the complete set-up was to replace the one inch posts, with two inch posts, but it was still not stable enough, see Fig. 4.13(a). Next try was to put four additional posts under the breadboard so that there were all in all nine two inch posts under the cavity, but it was still not stable enough, see Fig. 4.13(b). Another attempt was to put the cavity on a thicker vibration damping breadboard, but because of the insufficient space in the vacuum chamber just a thin breadboard could be used, and it was not stable enough, see 4.13(c). Next try was to fix the cavity directly to the optical table, this configuration was the first one which showed a promising stability see Fig. 4.13(d). This was quite surprising because the vibrations came from the table, but it seemed to be the posts which magnified the vibration and the thin breadboard could not damp them.

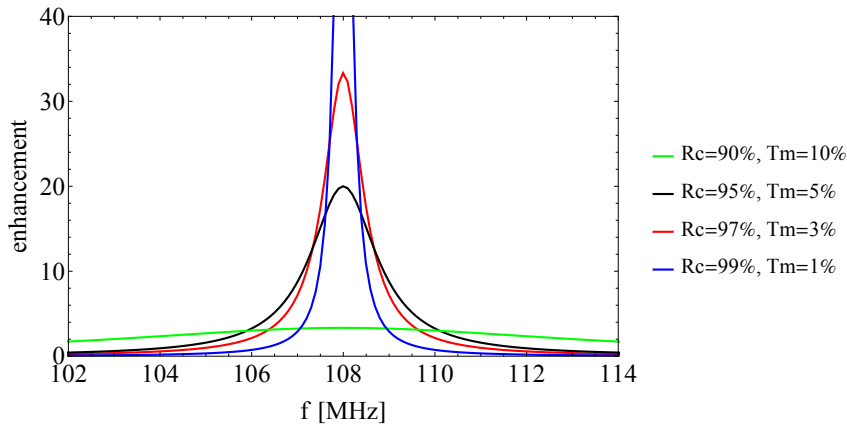


Figure 4.12: Cavity mode width depending on the enhancement. High enhancement leads to a narrow spectrum which is enhanced, low enhancement to a broadened spectrum which is enhanced.

This caused the instability of the cavity. The complete setup was rebuilt by mounting the vacuum chamber directly to the optical table and mount the cavity directly to the chamber. However it turned out that the chamber was not flat neither inside nor outside. Maybe if a new vacuum chamber is ordered it would be a good idea to make sure that it is flat inside and outside, to have better opportunities. A last desperate try was to put the cavity on twelve vibration damping rubber feet and just put it on the table without any attachment. Surprisingly it showed the best result of all tested setups, see Fig. 4.13(e). With the new awareness of vibration isolated cavity design and the given components, a new setup was constructed, see Fig. 4.14. The cavity-1, rests on twelve rubber feet-2, without any attachment to the vacuum chamber-3. The chamber is sealed with aluminium flanges-5, and with ten one inch posts-6 with a length of 25 mm, fixed with clamping jaws to a breadboard-4. The breadboard is necessary to get the correct height for the spectrograph. The breadboard also is clamped to the optical table.

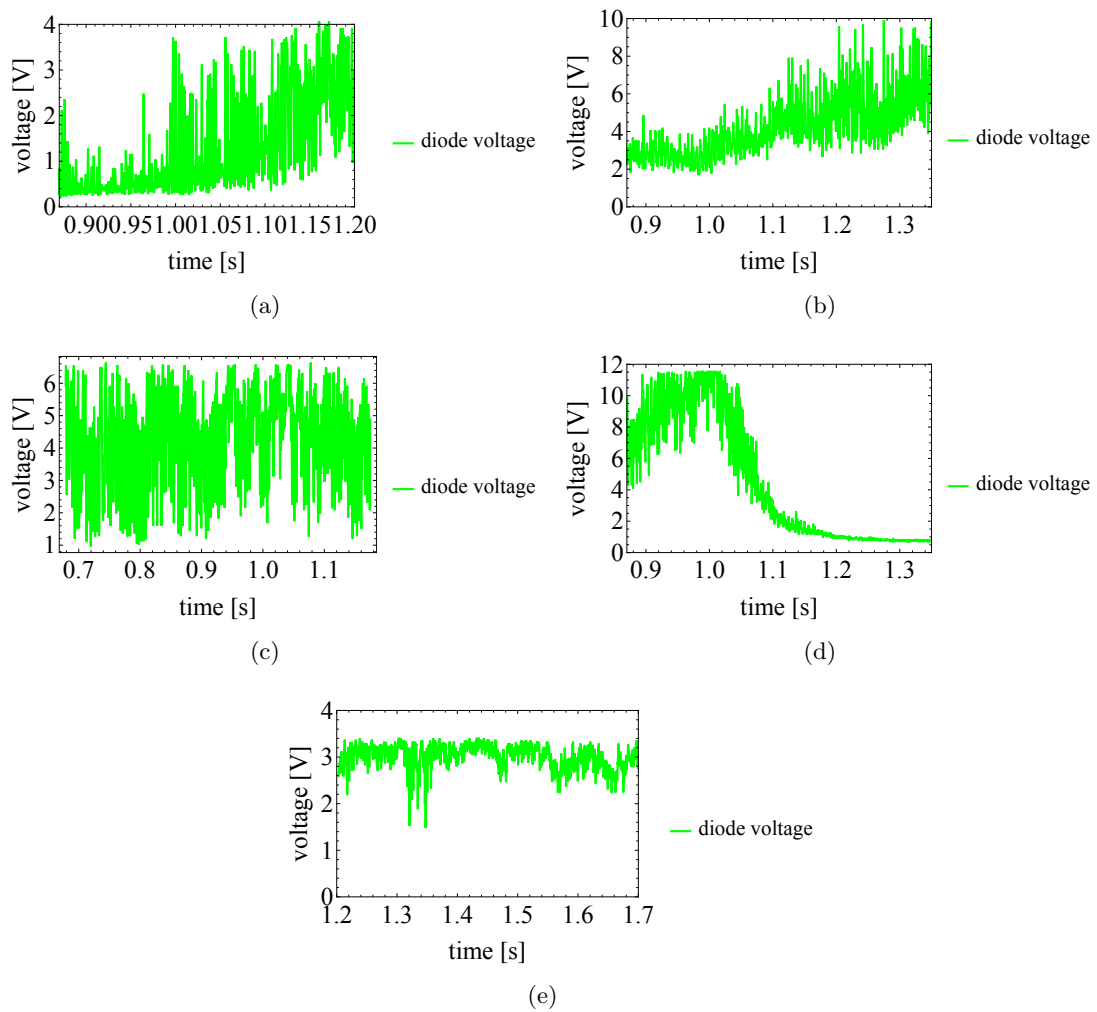
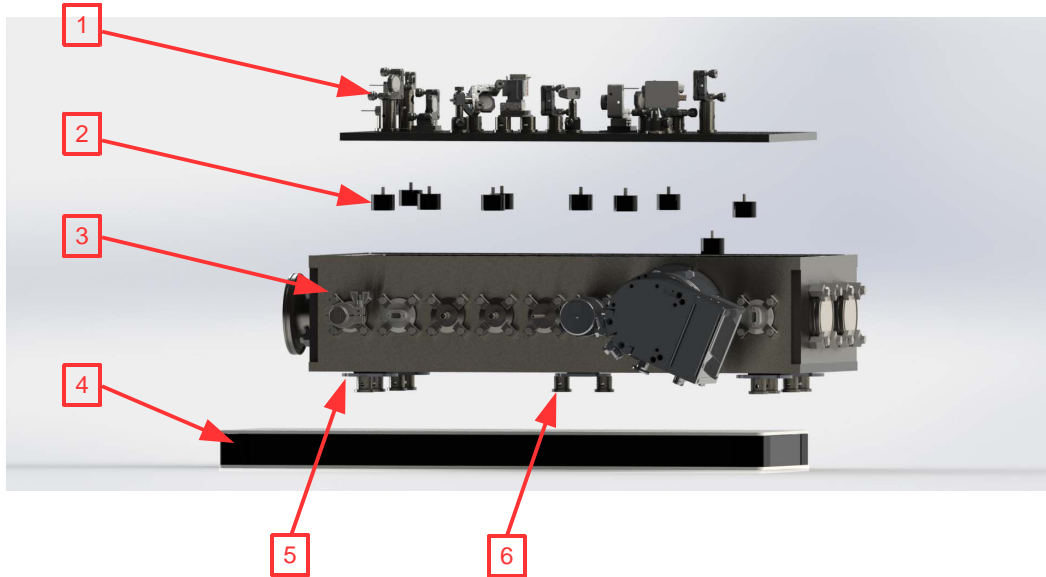
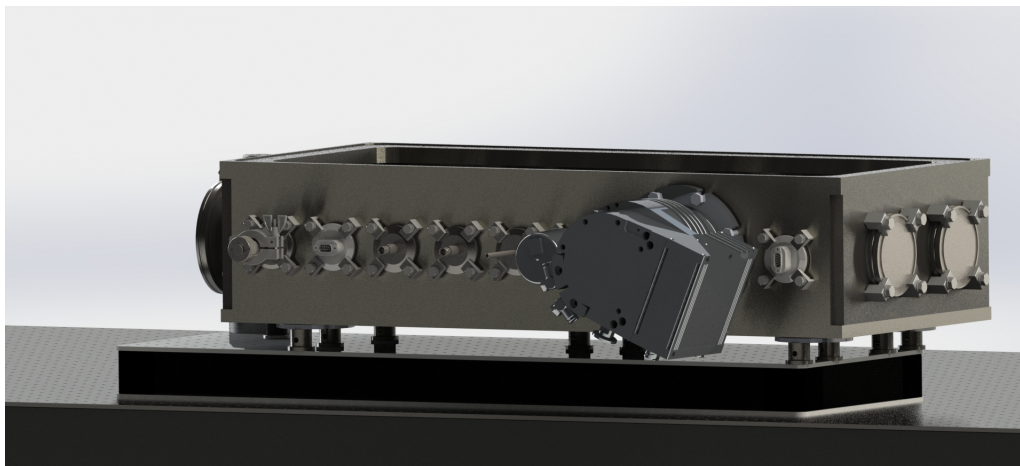


Figure 4.13: Stability of different cavity setups, cavity with five two inch posts (a), cavity with nine two inch posts (b), cavity with nine two inch posts and thicker breadboard (c), cavity mounted directly to the table (d), cavity with vibration damping rubber feet not fixed to the table (e).



(a)



(b)

Figure 4.14: Revised setup of the connection of the cavity with the vacuum chamber and the optical table. Exploded view (a), Composite configuration (b).

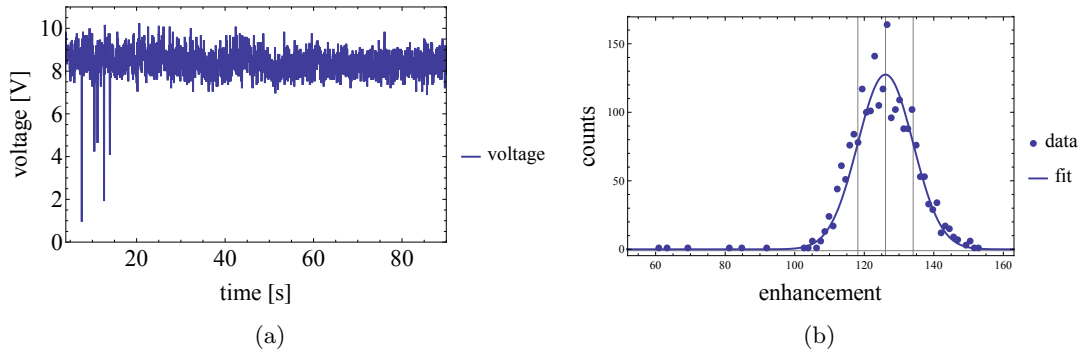


Figure 4.15: Stability of the cavity in the revised setup with a maximum enhancement of 150. Diode signal (a), distribution of the enhancement 4.15(b).

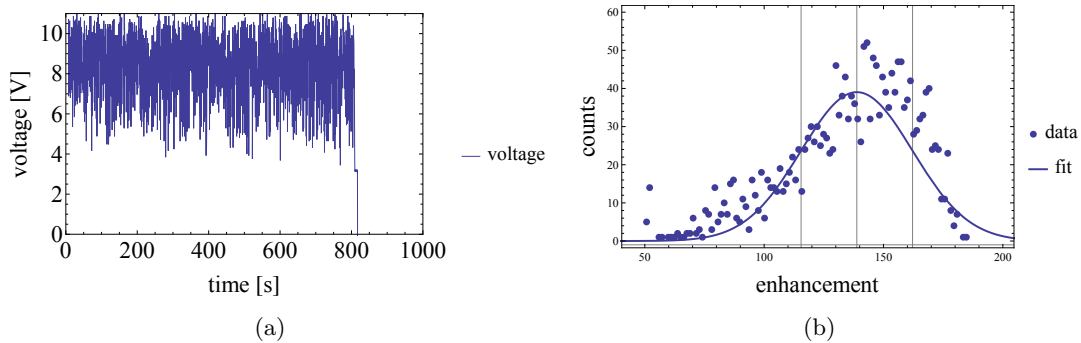


Figure 4.16: Stability of the cavity in the revised setup with a maximum enhancement of 180. Diode signal (a), distribution of the enhancement 4.16(b).

4.8 Final Stability and Possible Further Improvements

The stability of the revised setup with a maximum enhancement of about 150 can be seen in Fig. 4.15(a), note that maximum enhancement characterizes the highest enhancement which was detected during the measurement, the mean enhancement is smaller. The associated distribution of the enhancement during the stabilization can be seen in Fig 4.15(b). A Gauss function was fitted to the measuring data, the mean enhancement is 126 and the standard deviation is 8. Compared to the 100% fluctuation with an enhancement of 100, as it occurred in the original setup, this is a huge improvement. With the reconditioned 3D-Cavity, where the in-coupling-mirror possess a reflectivity of 0.5% a maximum enhancement of 180 is reached. This is in accordance with the calculation in Sec.2. It is possible to stabilize the cavity on resonance, for about 15 minutes by using a Hanch Couillaud setup, see Fig. 4.16(a). The associated distribution of the enhancement during the stabilization can be seen in Fig 4.16(b). Again a Gauss function, see Eq. 4.1, was fitted. The fitted curve shows a mean enhancement of 139 and a standard deviation of 23. The Hanch Couillaud setup drives a mirror which is glued to a Piezo. This compensates the length changes of the cavity caused by vibrations, ther-

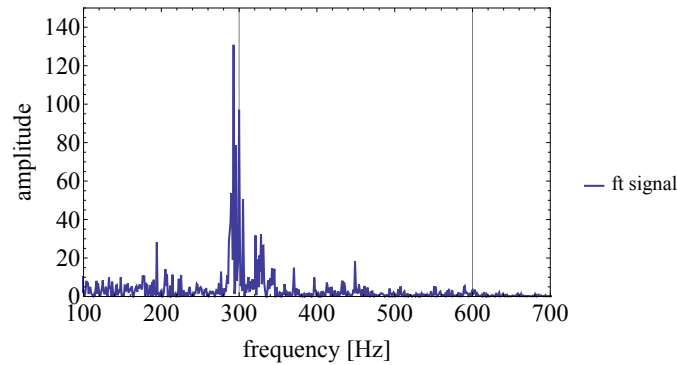


Figure 4.17: Fourier analysis of the diode signal of the revised cavity, a significant peak at 300 Hz still can be seen.

mal fluctuation and pressure changes. The Piezo which was used in this setup, shows a movement range of approximately 100 nm. This movement range is not sufficient for long term stabilization, therefore it is necessary to move the translation stage with the mirror mounted on it, to keep the Piezo still in range. Unfortunately, this is not possible because the used translation stages do not provide small enough steps to keep the cavity in lock. The used translation stages see A.8, according to the user manual, have a minimum step size of 50 nm. In one direction 50 nm steps are possible, in the other direction the step size is larger. However, it was not possible to move the translation stage and keep the cavity still in lock with the smallest possible step size. Note, that in the direction of the smaller step size it was sometimes possible. Unfortunately, the used translation stages have the smallest minimum incremental motion of the Newport Agilis series. This means that if a translation stage is exchanged by a stage with a smaller minimum step size it has to be from another series, or company, and the complete control electronics and programs have to be exchanged. It would also be possible to use a Piezo with a larger movement range but one has to make sure that this Piezo does not enhance the instability of the complete setup.

In the Fourier-transform of the diode signal the 300 Hz perturbation is still detectable, especially for high enhancement, even if the amplitude is much lower, see figure 4.17. The new setup damps this vibration, but does not completely isolate the cavity from it. The cavity is still sensitive to vibrations occurring in the lab like walking, loud talking and opening/closing of a door. This is a clear sign that the vibration isolation still has to be improved. Possibly by using a minus-K vibration isolation table and an acoustic isolation around the experiment. The complete experiment should be designed to be controlled from outside the lab to generate as less perturbations as possible.

Furthermore, at the moment the comb offset can be stabilised only to a given value set by the production company and unfortunately it was not possible to reach high enhancement with a locked comb offset. The drift of this offset influences the enhancement and the stability of the cavity dramatically. Maybe there is the possibility of getting a software update for the frequency comb to lock the offset to any number, but at least

the linear dispersion should be compensated. This can be done by using two wedges in the beam between the comb and the cavity controlled by an additional Hänch Couillaud setup. Unfortunately, this adds more dispersion to the beam which also has to be compensated.

However the critical value for the stability of the cavity during the high harmonic generation process is the rising gas pressure in the cavity which comes from the Xenon which is sent into the laser beam. The used vacuum pump, a HiPace300M turbo molecular vacuum pump, see A.11 is not efficient enough to keep the pressure constant for the given gas jet design and the gas pressure which is used for the high harmonic generation. This can be improved by a new, smaller gas jet design, exchanging the pump with a better one, adding additional vacuum pumps, or a special gas containment in the cavity. Note that more material in the cavity generates more losses and influences the enhancement dramatically.

The gas jet is mounted on a 3D-translation stage to align the jet to the cavity focus. This construction is quite heavy and has to be moved a lot during the experiment to find the correct position, therefore the 3D-stage should not be mounted on the breadboard. Another source for vibrations are the cables which were needed to control the translation stages, the photo diode and the camera. They were mounted directly to the vacuum chamber. To damp vibrations they should be mounted to a construction which is not connected to the optical table and only with very thin and flexible wires connected to the vacuum chamber.

5 th Harmonic

[..] und es ward Licht.

As discussed in Sec. 1.3, an intensity of $10^{13} \text{ W/cm}^2 \sim 10^{14} \text{ W/cm}^2$ is needed for high harmonic generation [8]. With the cavity setup which was built during this master thesis it is possible to reach an enhancement e_h of 180, a focus size of ω_{f1} , of $12 \mu\text{m}$, an input power I_i of 950 mW, and a pulse duration Δt of 40 fs. With a repetition frequency f_{rep} of 108 MHz one can calculate the intensity of the cavity focus f_1 by:

$$I_{f1} = \frac{e_h I_i}{\omega_{f1} \Delta t f_{rep}} \approx 10^{13} \frac{W}{cm^2}. \quad (5.1)$$

This means that it should be possible to generate 3rd and 5th harmonics in Xenon. Figure 5.1 shows a spectral scan of the wavelength of the light which is coupled out of the cavity, spectrally resolved with a grating and detected with a photomultiplier. As it can be seen there is light at the 3rd harmonic (266 nm) and also at the 5th harmonic (160 nm). A filter was used to reduce the much stronger 3rd harmonic and also the zero order 800 nm light. The signal at 160 nm is close to the edge of the resolution of the photomultiplier. Next step is to optimise the signal. Theoretically the intensity should be high enough and there should be more generated high harmonic light. Therefore the first thing to improve is the out-coupling efficiency. Another option is to make the intra-cavity focus even smaller by changing the cavity mirrors to a radius of $R = 50 \text{ mm}$. Further work also will be to analyze the signal to see if it still has a comb structure. In this thesis it could be established that the setup generates light in the 160 nm regime.

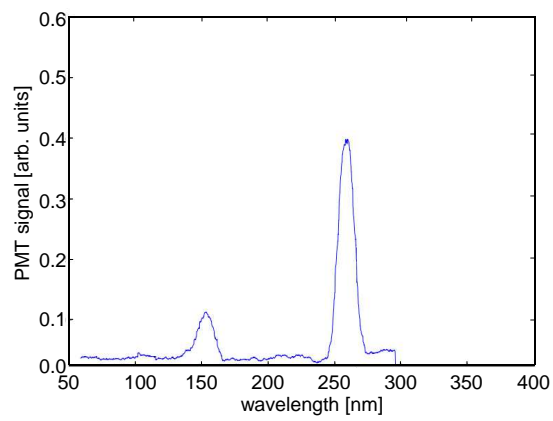


Figure 5.1: Spectral scan over the light which is coupled out and analyzed with a spectrometer and a photomultiplier. The signal of the 3rd harmonic (266nm) and the 5th harmonic (160nm) is clearly visible.

6 Summary and Outlook

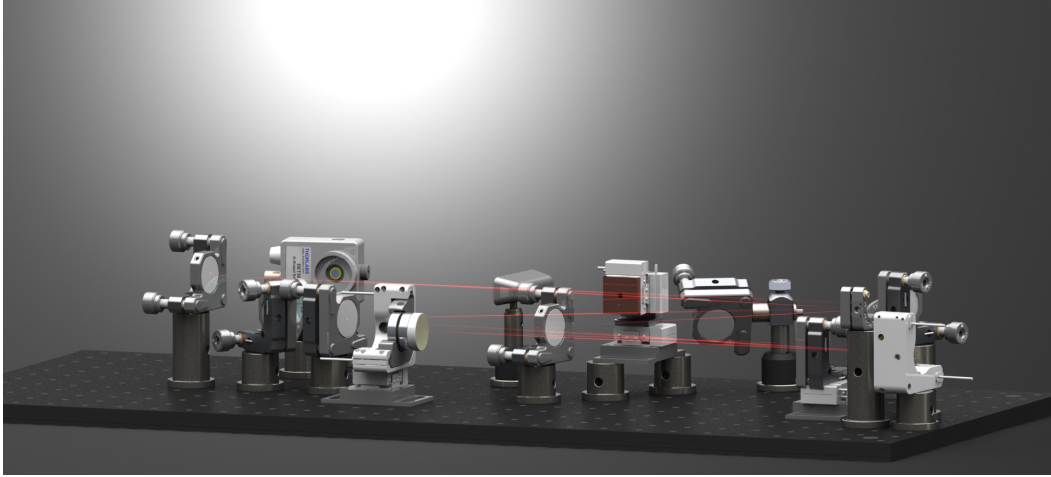


Figure 6.1: 3D-cavity

During this master thesis it is shown that by using a 3D-enhancement cavity design, see Fig. 6.1, the complete stability range of the cavity can be used and thus a smaller intra-cavity focus can be achieved. It has also been shown theoretically and experimentally that the length of this type of cavity can be stabilized on resonance by using the Hänch Couillaud stabilization setup. Furthermore, it is also theoretically proven that the linear dispersion in the cavity can be compensated by using two wedges and a second Hänch Couillaud setup. The optical table collects noise from the laboratory and on the surface of the table a vibration of 360 Hz is measured with an acceleration sensor. The first implemented vibration isolating setup isolates the cavity quite well from the vibrations of the vacuum pumps but not from the vibrations of the optical table. After a lot of testing it turned out that an unattached cavity on vibration damping rubber feet works best and with the existing components a new setup was built. The new setup is a compromise between using the existing parts to save time and money and what is the best for vibration isolation. For similar experiments or further rebuilds there are a lot of things one can do better. The lab should be acoustically isolated. There should be as little noise as possible in the lab, in contrast to the actual used pre vacuum pumps which are extremely loud. The next setup should improve the isolation of the cavity from vibrations of the optical table by a special damping element, for example the minus-K vibration isolation tables. The best way would be to use such a table in vacuum. However, the improved setup could be stabilized for about 15 minutes on resonance with a maximal enhancement of 180, and it was possible to generate light with a wavelength of 160 nm by generating 5th harmonics in Xenon.

Bibliography

- [1] B. R. Beck; J. A. Becker; P. Beiersdorfer; G.V. Brown; K. J. Moody; J. B. Wilhelmy; F. S. Porter; C. A. Kilbourne; and R. L. Kelley. “Energy Splitting of the Ground-State Doublet in the Nucleus ^{229}Th ”. In: *Physical Review Letters* PRL 98 (6 April 2007), (142501–1)–(142501–4).
- [2] E. Peik and Chr. Tamm. “Nuclear laser spectroscopy of the 3.5 eV transition in Th-^{229} ”. In: *Europhysics Letters* 61 (2003).
- [3] Joachim Pupeza. *Power Scaling of Enhancement Cavities for Nonlinear Optics*. Ed. by Max-Planck-Institut fuer Quantenoptik. Oktober 2011.
- [4] Joerg Reichert. *Praezise optische Frequenzmessungen mit modengekoppelten Lasern*. Ed. by Ludwig Maximilians Universitaet Mueunchen. 2000.
- [5] Dylan Yost. *Development of an Extreme Ultraviolet Frequency Comb for Precision Spectroscopy*. Ed. by University of Colorado. 2008.
- [6] Christoph Gohle. *A Coherent Frequency Comb in the Extreme Ultraviolet*. Ed. by LudwigMaximiliansvUniversitaet. 21. Maerz 2006.
- [7] David J. Jones; Scott A. Diddams; Jinendra K. Ranka; Andrew Stentz; Robert S. Windeler; John L. Hall; Steven T. Cundiff. “Carrier-Envelope Phase Control of Femtosecond Mode-Locked Lasers and Direct Optical Frequency Synthesis”. In: *Science* 288 (28 AprilL 2000), pp. 635–639.
- [8] I. A. McIntyre; K. Boyer; A. McPherson; G. Gibson H. Jara; U. Johann; T. S. Luk and C. K. Rhodes. “Studies of multiphoton production of vacuum-ultraviolet radiation in the rare gases”. In: *J. Opt. Soc. Am B* 4 (April 1987), pp. 595–601.
- [9] M. Lewenstein; Ph. Balcou; M. Yu. Ivanov; Anne L’Huillier; and P. B. Corkum. “Theory of high-harmonic generation by low-frequency laser fields”. In: *Physical Review* 49, Number 3 (March 1994), pp. 2118–2132.
- [10] Anton Husakou Usman Sapaev and Joachim Herrmann. “Combined action of the bound-electron nonlinearity and the tunnel-ionization current in low-order harmonic generation in noble gases”. In: *Optics Express* 21 (21 October 2013), pp. 25582–25591.
- [11] Yohei Kobayashi; Nozomi Hirayama; Akira Ozawa; Takashi Sukegawa; Takashi Seki; Yoshiyuki Kuramoto; and Shuntaro Watanabe. “10-MHz, Yb-fiber chirped-pulse amplifier system with large-scale transmission gratings”. In: *Optics Express* 21 (17 May 2013), p. 1286512873.
- [12] Ingolf V. Hertel und Claus-Peter Schulz. *Atome im starken Laserfelder*. Ed. by Springer. 31. Oktober 2010.
- [13] Max Born and Emil Wolf. *Principles of Optics*. Ed. by Pergamon Press. Fourth Edition. Oxford, 1970.

- [14] Orazio Svelto. *Principles of Lasers*. Ed. by Springer. Fourth Edition. 1970.
- [15] R. Jason Jones and Jun Ye. “High-repetition-rate coherent femtosecond pulse amplification with an external passive optical cavity”. In: *Optics Letters* (2004).
- [16] H. Kogelnik and T. Li. “Laser Beams and Resonators”. In: *Applied Optics* 5, No.10 (October 1966), pp. 1550–1567.
- [17] Herwig W.Kogelnik; Erich P.Ippen; Andrew Dienes; Charls V.Shank. “Astigmat-ically Compensated Cavities for CW Dye Lasers”. In: *Ieee JournalL of Quantum Electronic* (March 1972), pp. 373–379.
- [18] Hansch and B. Couillaud. “Laser Frequency Stabilization by Polarization Spec-troscopy of a Reflecting Reference Cavity”. In: *Optics Communications* 3 35 (De-cember 1980), pp. 442–444.

A Components

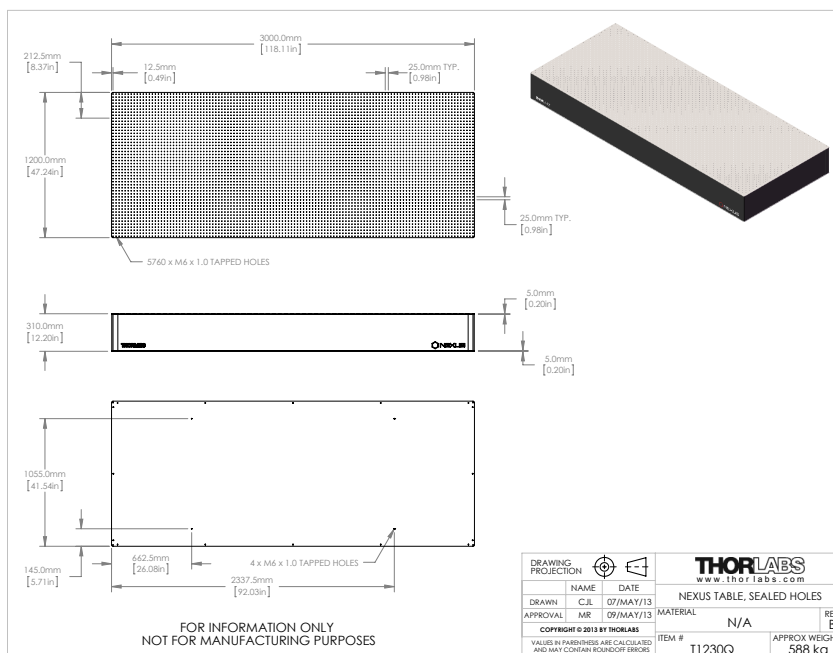


Figure A.1: Optical table

FC8004

Optical Frequency Synthesizer



The FC8004 Optical Frequency Synthesizer gives the user access to optical frequency measurement techniques with unprecedented accuracy and flexibility. This novel, extraordinary precise technology can be implemented in applications such as frequency chain generation, optical atomic clocks and ultra high precision spectroscopy. It has been successfully field tested in many laboratories worldwide. The Optical Frequency Synthesizer technology is based on a femtosecond laser frequency comb. It requires the stabilization of two important parameters: Repetition rate ω_r and offset frequency ω_o . From the exact knowledge of these two radio frequencies one can derive the optical frequency of any mode $\omega_n = n\omega_r + \omega_o$.

MenloSystems

KEY SPECIFICATIONS

- Comb Spacing 200 MHz
- Accuracy Better 10^{-14}
- Stability Better 5×10^{-13} in One Second

APPLICATIONS

- High Precision CW Laser Stabilization
- FTIR Spectroscopy
- Calibration of Laser

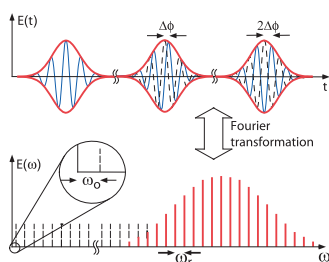
FEATURES

- Ti:Sa Oscillator
- Turnkey Metrology System Fully Automated with Comb Control and Data Acquisition Software

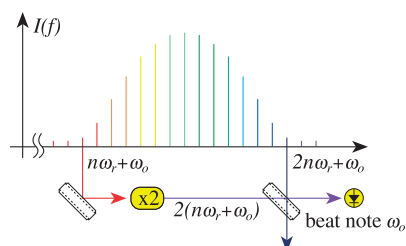
OPTIONS

- **BDU** beat detection unit with free space or fiber-coupled optics.
- **GPS-10** GPS based 10 MHz reference

OPERATION PRINCIPLE



Consecutive pulses of the pulse train emitted by a mode locked laser and the corresponding spectrum. The carrier wave (shown in blue) shifts by $\Delta\phi$ after each round trip with respect to the pulse envelope (shown in red). This continuous shift results in a frequency offset $\omega = \Delta\phi/T$ of the comb.



Stabilization of the offset frequency and the pulse to pulse phase slippage by frequency doubling the infrared part of the comb and observation of the beat with the blue part.

Figure A.2: Frequency comb.

FC8004



Optical Frequency Synthesizer

SPECIFICATIONS

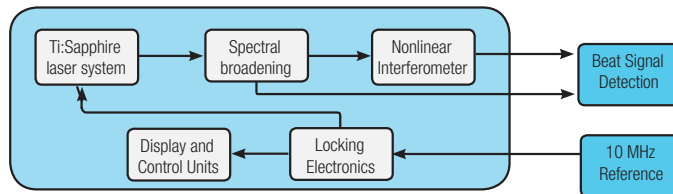
Comb Spacing	200 MHz	
Accuracy	10 ⁻¹⁴ or same as reference*	
Stability	5x10 ⁻¹³ in 1 s or same as reference*	
Accessible Spectral Range	Output Port 1: 630-850 nm	Output Port 2: 532, 1064 nm

* whichever applies first

REQUIREMENTS

Input Requirements	10 MHz frequency reference, power level +7 dBm	
Operating Voltage	100/115/230 VAC	
Frequency	50 to 60 Hz	

SCHEMATIC SETUP



ORDERING INFORMATION

Product Code	FC8004
--------------	--------

Please call for pricing. Specifications are subject to change without notice. Custom modifications are available, please inquire.



Invisible laser radiation
avoid exposure to beam
Class 4 laser



Menlo Systems GmbH
T+49 89 189 166 0
sales@menlosystems.com

Menlo Systems, Inc.
T+1 973 300 4490
ussales@menlosystems.com

Thorlabs, Inc.
T+1 973 579 7227
sales@thorlabs.com



www.menlosystems.com

www.frequencycomb.com

D-FC8004-EN 29/07/14

Figure A.3: Frequency comb.

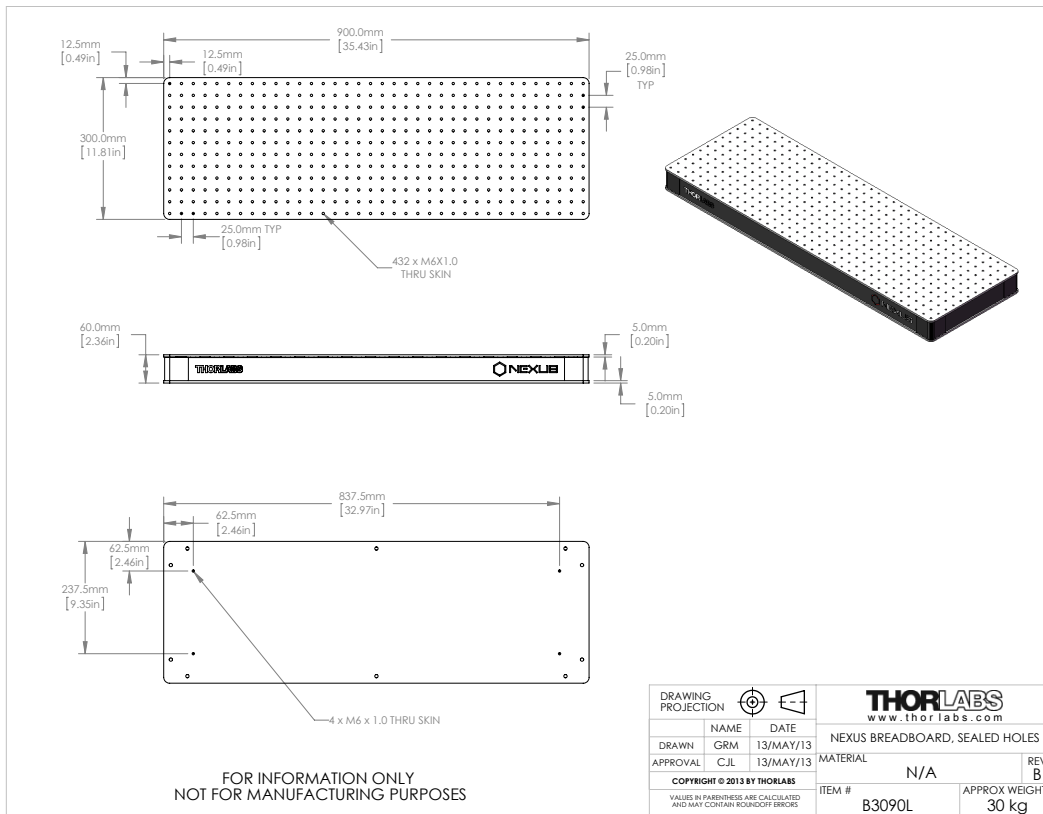


Figure A.4: Breadboard.

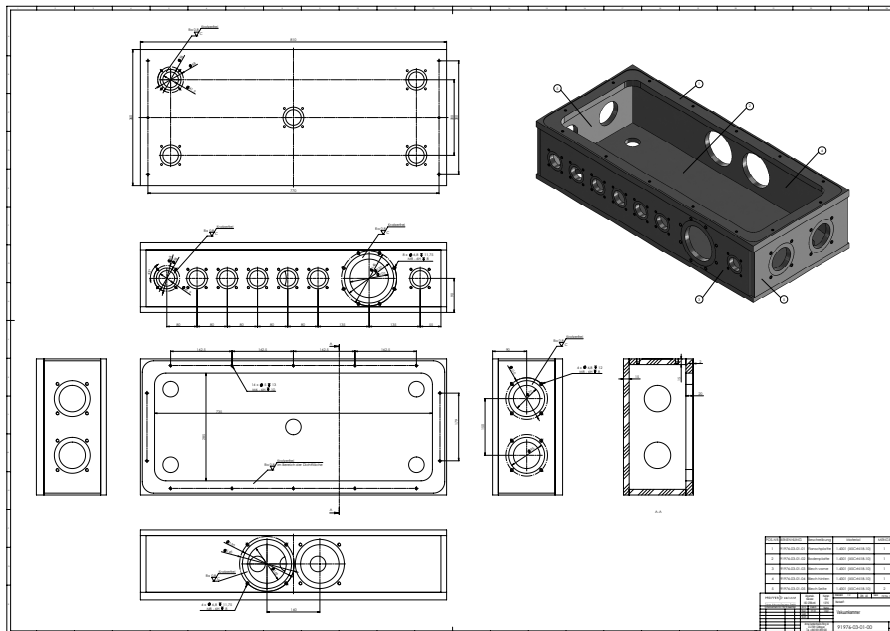


Figure A.5: Vacuum chamber.

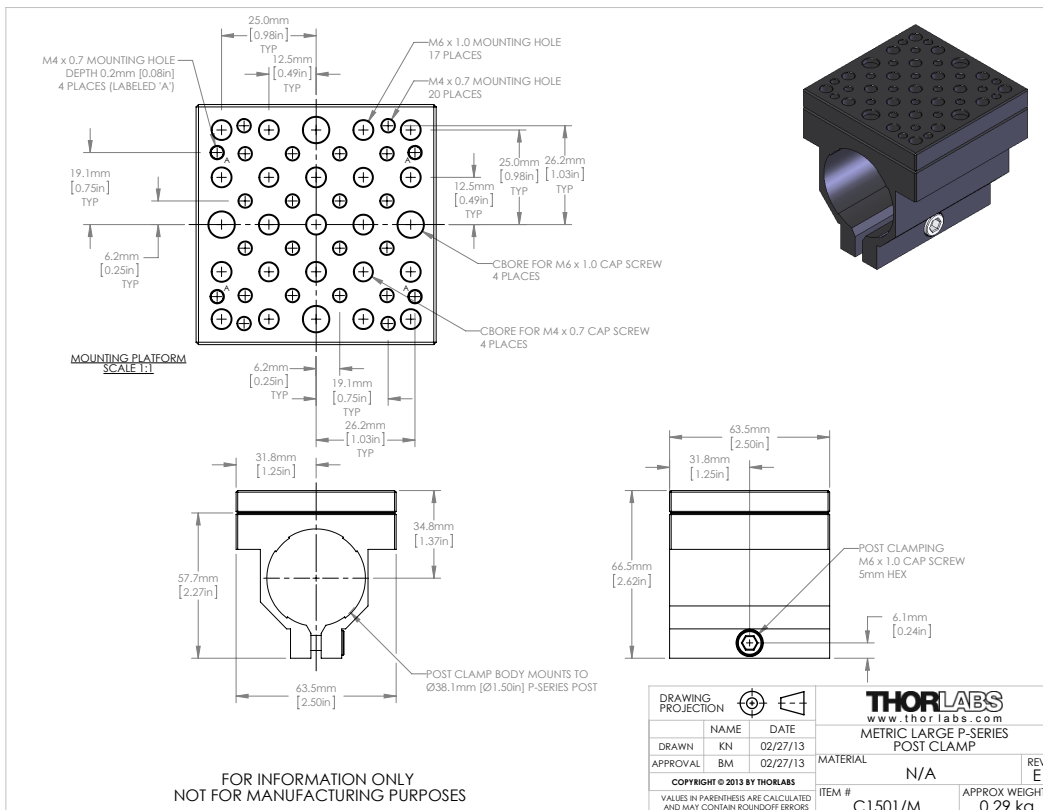
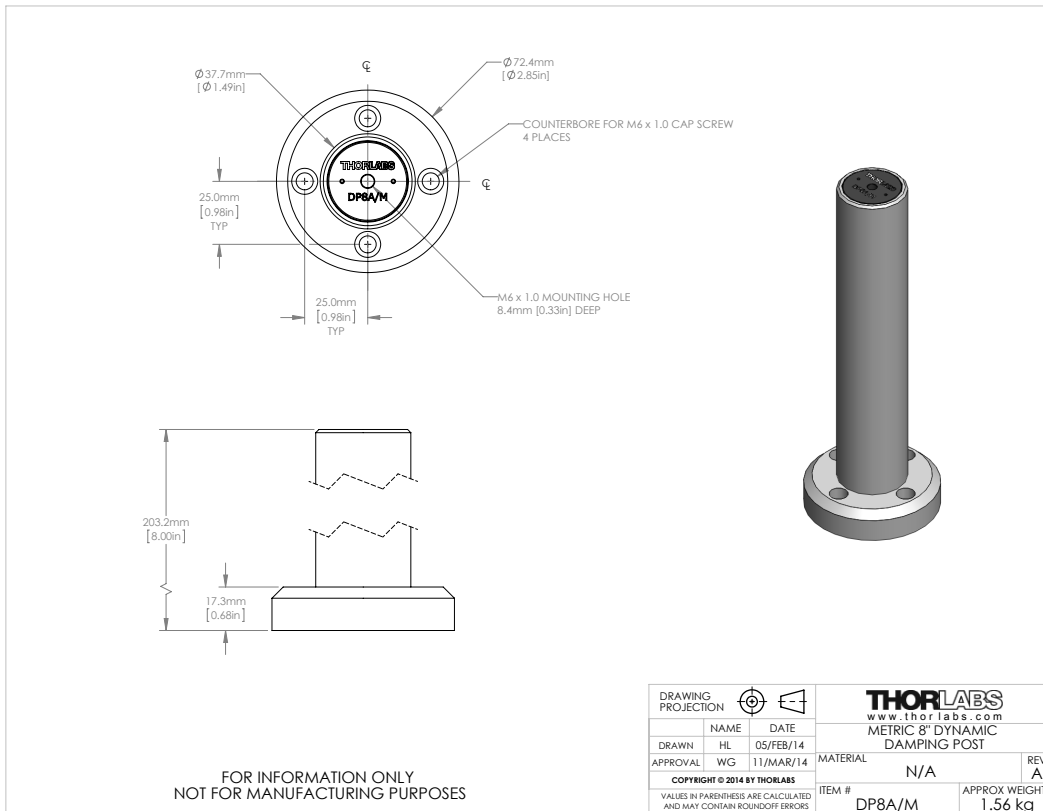


Figure A.6: Vibration damping post.

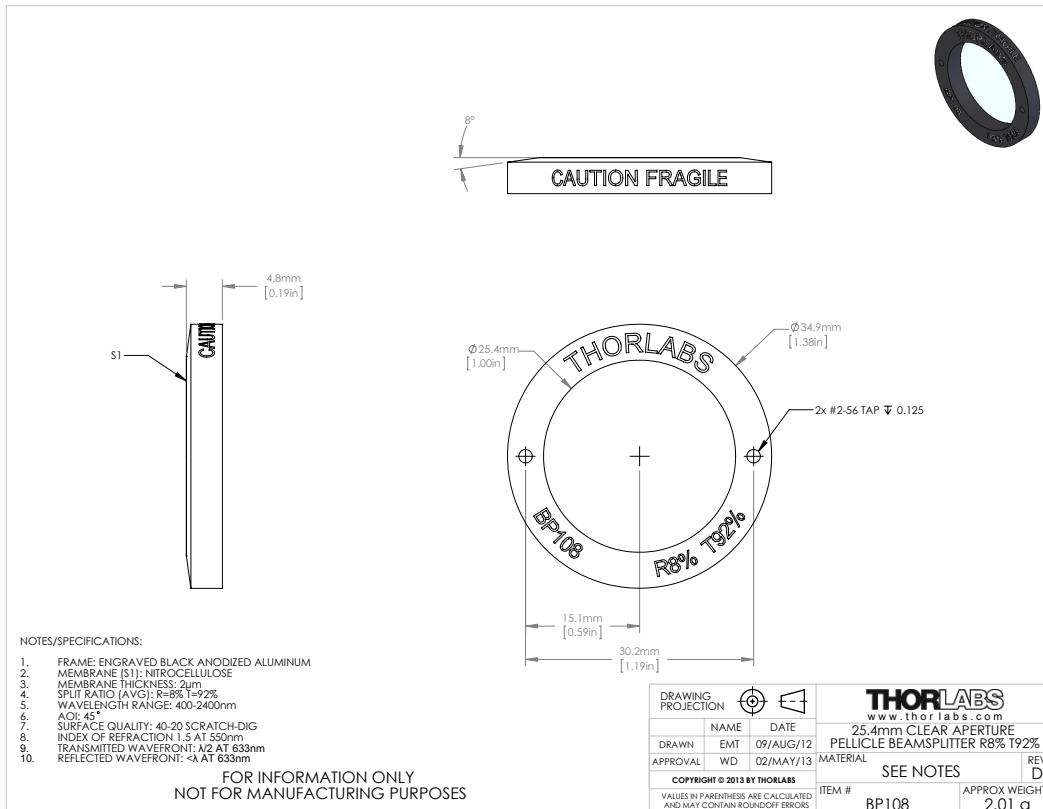


Figure A.7: BP108.

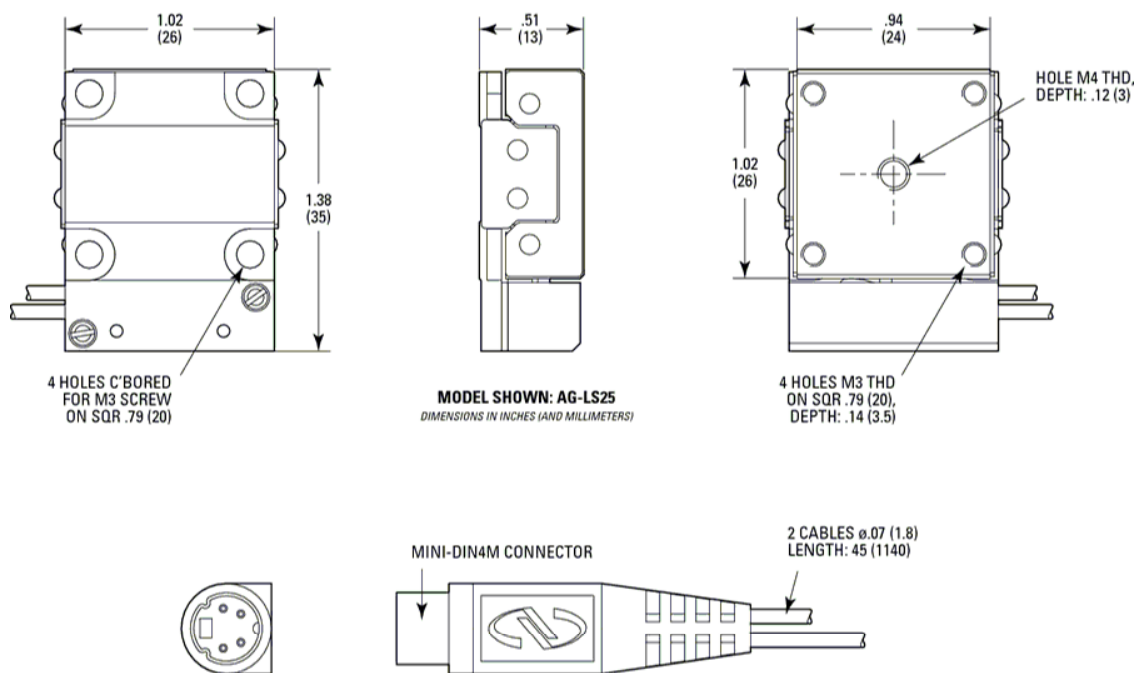


Figure A.8: Newport Agilis Series AG-LS25 Piezo-Motor-Driven-Linear-Stage.

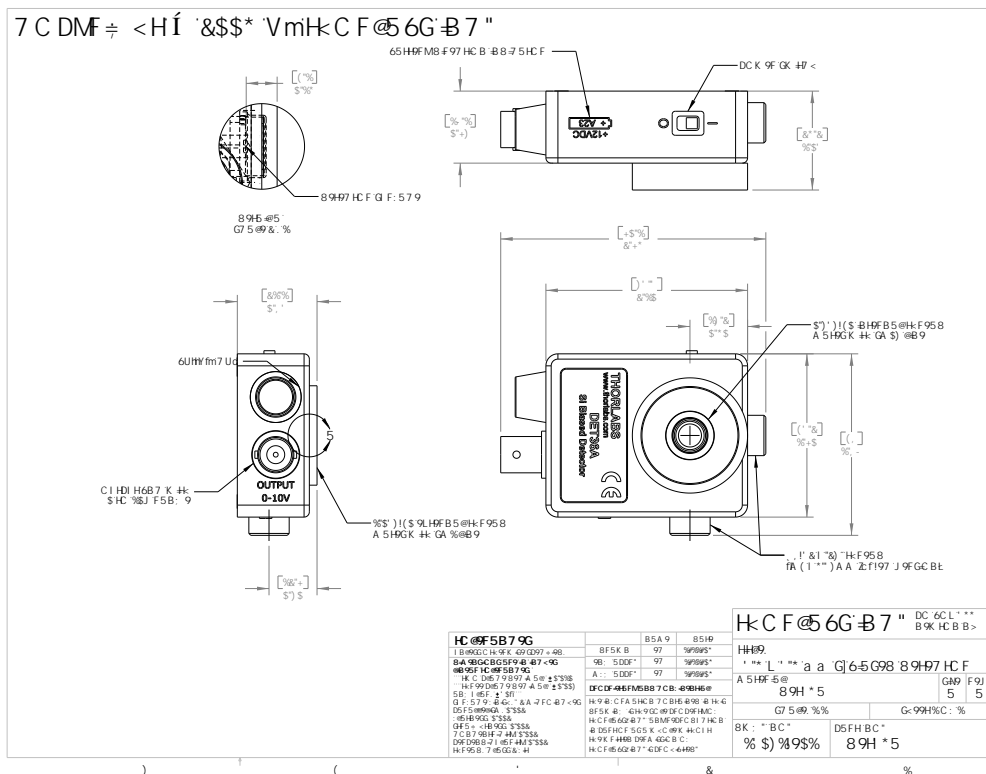


Figure A.9: Photodiode.

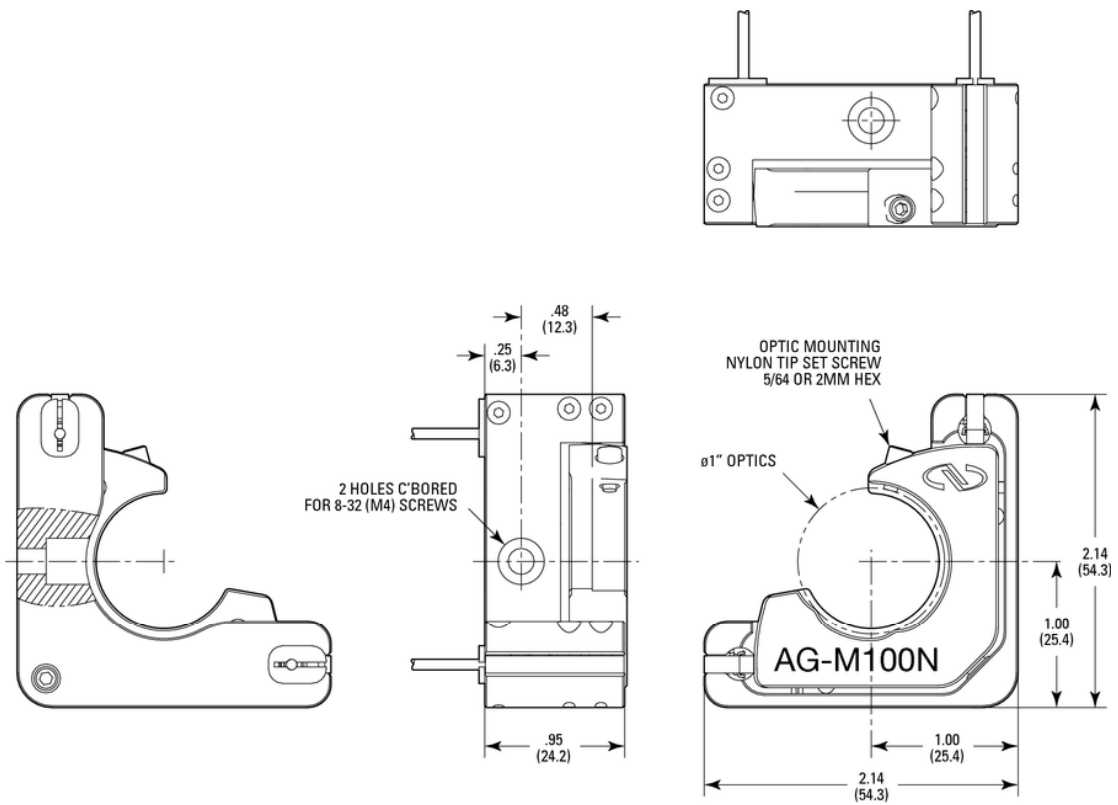


Figure A.10: Newport Agilis Series AG-M100N Piezo Motor Driven Optical Mount.

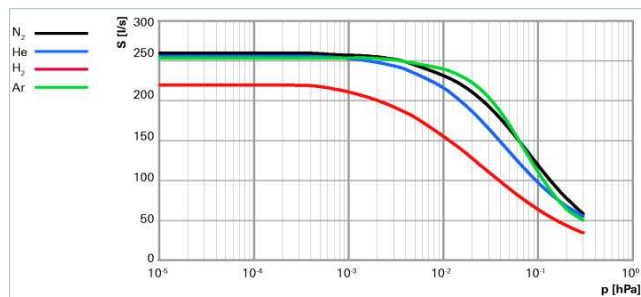


Abbildung ähnlich

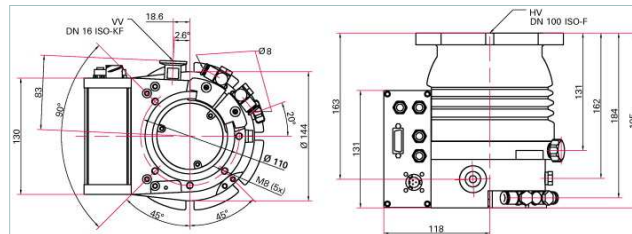
HiPace® 300 mit TC 400, DN 100 ISO-F

- Robuste, leistungsstarke Turbopumpe mit einem Saugvermögen bis zu 260 l/s für N₂
- Integrierte Antriebselektronik TC 400
- Ideal für Analytik und industrielle Applikationen
- Für den Einbau in allen Lagen
- Mit integrierter Wasserkühlung für maximalen Gasdurchsatz
- Flexibel durch Einsatz von bis zu 4 Zubehörtellen
- Ideal für schnelle Zyklen
- Umfangreiches Zubehör erweitert das Anwendungsspektrum

C=Korrosivgasversion



Maßbild



Technische Daten	HiPace® 300 mit TC 400, DN 100 ISO-F
Anschlussflansch (Ausgang)	DN 16 ISO-KF / G 1/4"
Anschlussflansch (Eingang)	DN 100 ISO-F
Antriebselektronik	mit TC 400
Betriebsspannung	24 (± 5 %) V DC
Drehzahl ± 2 %	60000 min ⁻¹
Drehzahl variabel	35-100 %
Einbaulage	Allelagen
Enddruck gemäß PNEUROP	< 1 · 10 ⁻⁷ hPa < 7,5 · 10 ⁻³ Torr < 1 · 10 ⁻⁷ mbar
Flutanschluss	G 1/8"
Gasdurchsatz bei Enddrehzahl für Ar	7 hPa l/s 5,25 Torr l/s 7 mbar l/s
Gasdurchsatz bei Enddrehzahl für H ₂	> 14 hPa l/s > 10,5 Torr l/s > 14 mbar l/s

Figure A.11: Pfeiffer-Vacuum turbo molecular vacuum pump HiPace 300.